JQS **Journal of Quaternary Science** **QRA**
Quaternary Research Association

Millennial-scale shifts in microtidal ecosystems during the Holocene: dynamics and drivers of change from the Po Plain coastal record (NE Italy)

VERONICA ROSSI,[1] GIULIA BARBIERI,[1]* STEFANO CLAUDIO VAIANI,[1] MARCO CACCIARI,[1] LUIGI BRUNO,[2] BRUNO CAMPO,[1] MARCO MARCHESINI,[3] SILVIA MARVELLI[3] and ALESSANDRO AMOROSI[1]
[1]Department of Biological, Geological and Environmental Sciences, University of Bologna, Italy
[2]Department of Chemical and Geological Sciences, University of Modena and Reggio Emilia, Italy
[3]Laboratory of Palinology and Archaeobotany, C.A.A. – Giorgio Nicoli, Italy

ABSTRACT: Framed into a robust stratigraphic context, multivariate analyses on the Holocene palaeobiological record (pollen, benthic foraminifers, ostracods) of the Po coastal plain (NE Italy) allowed the investigation of microtidal ecosystems variability and driving parameters along a 35-km-long land–sea transect. Millennial-scale ecosystem shifts are documented by coeval changes in the meiofauna, reflecting variations in organic matter–water depth (shallow-marine environments) and degree of confinement-salinity (back-barrier settings). In-phase shifts of vegetation communities track unsteady water-table levels and river dynamics in freshwater palustrine areas. Five environmental–ecological stages followed one another crossing four tipping points that mark changes in relative sea level (RSL), climate and/or fluvial regime. At the culmination of Mediterranean RSL rise, after the 8200 event, remarkable growth of peatlands took place in the Po estuary, while low accumulation rates typified the shelf. At the transgressive–regressive turnaround (~7000 cal a BP), the estuary turned into a delta plain with tidally influenced interdistributary embayments. River flow regime oscillations after the Climate Optimum (post-5000 cal a BP) favoured isolation of the bays and the development of brackish wetlands surrounded by wooded peatlands. The youngest threshold (~800 cal a BP), which led to the establishment of the modern delta, reflects a major avulsion of the Po River. © 2021 The Authors. *Journal of Quaternary Science* Published by John Wiley & Sons Ltd.

KEYWORDS: climate change effects; Holocene; Mediterranean wetlands; meiofauna; pollen

Introduction

Deltas, coastal lagoons, estuaries and adjacent areas, including freshwater swamp/marshes and beach barriers, are considered valuable environments and ecosystems that deserve to be protected and preserved under the threat of Global Change (Alizad et al., 2018; Aucelli et al., 2018). These areas play a strategic role in protection of lowlands against natural hazards (e.g. floods, storms, hurricanes), carbon accumulation/storage and biodiversity preservation (e.g. Shepard et al., 2011; Rogers et al., 2019). Besides, coastal wetlands host a wide range of ecosystem services (e.g. food availability, freshwater supply, conveyances of goods and people) that have been exploited by humans since prehistorical times (e.g. Balbo et al., 2017), as testified to by the presence of several archaeological sites, particularly along the Mediterranean coasts (e.g. Ghilardi et al., 2017; Giaime et al., 2019; Reimann et al., 2018). However, the transitional state between terrestrial and marine realms associated with the low-elevation, flat morphologies and high subsidence rates make these environments extremely susceptible to even subtle changes in relative sea level (RSL) and fluvial activity (e.g. Simeoni and Corbau, 2009; Perini et al., 2017). Both parameters are, in turn, potentially influenced by natural (e.g. climate, vegetation and river dynamics) and anthropic (e.g. CO$_2$ emissions, river regulations, reclamations) factors operating at various scales through space and time. Due to such a complex scenario, the response of coastal wetlands to Global Change remains uncertain and all controlling factors (e.g. rates of RSL rise,

accommodation, sediment input, biophysical processes, anthropogenic structures) should be considered to produce reliable projections of future evolution (Schuerch et al., 2018).

A geological perspective is key for addressing this issue and stratigraphic studies can provide a long-term view, useful for conservation and restoration strategies. In this respect, the subsurface sedimentary successions of the Mediterranean coastal plains represent invaluable archives containing the full set of bio-sedimentary data able to provide insights on past ecosystem dynamics and associated forcing (Leorri et al., 2006; Sacchi et al., 2014; Zecchin et al., 2014; Di Rita et al., 2015; Bellotti et al., 2016; Cearreta et al., 2016; Ejarque et al., 2016; Milli et al., 2016; Rodríguez-Pérez et al., 2018; Revelles et al., 2019; Seeliger et al., 2019; Vella et al., 2019). The integration of different fossil groups (e.g. molluscs, ostracods, benthic foraminifers, palynomorphs, diatoms) proved to be extremely successful for an improved facies characterization and detailed palaeoenvironmental reconstructions relying on several parameters (water depth/level, salinity, organic matter availability, oxygen content and substrate conditions). Among others, ostracods and benthic foraminifers (i.e. the meiofauna) show very high ecological sensitivity in almost all aquatic habitats and a remarkable abundance within cored successions (e.g. Debenay and Guillou, 2002; Frenzel and Boomer, 2005; Murray, 2006; Horne et al., 2012). By contrast, pollen and spores are considered valuable indicators of past vegetation communities and their stratigraphic record is able to track simultaneously palaeoenvironmental, palaeoclimate and land-use changes (Bertini et al., 2010; Sadori, 2013; Mander and Punyasena, 2018).

*Correspondence: G. Barbieri, as above.
E-mail: giulia.barbieri21@unibo.it

A research approach that integrates ostracods, benthic foraminifers and palynomorphs is quite rare in the literature (Sadori *et al.*, 2016; Melis *et al.*, 2018; Kaniewski *et al.*, 2018; D'Orefice *et al.*, 2020) and has been applied to Holocene successions developed within one depositional setting (e.g. lagoon, wetland, coastal lake). To the best of our knowledge, a holistic perspective integrating faunistic and palynological data along a sea–land transect is still lacking.

The main purpose of this study is to provide high-resolution, multivariate data for a better comprehension of the dynamics of microtidal ecosystems ('one physical systems' *sensu* Tansley, 1935; Richter and Billings, 2015) under changing RSL and fluvial activity conditions, evaluating the Holocene variability/turnover from the sea to the innermost portion of the coastal zone. In this regard, the Po delta–coastal plain (NE Italy; Fig. 1) represents a key microtidal system in the Mediterranean basin, as it contains a series of prominent features: (i) a long-term growth of wetlands favoured by a rapidly subsiding setting (Bruno *et al.*, 2020); (ii) an advanced knowledge of the deltaic evolution (Correggiari *et al.*, 2005; Stefani and Vincenzi, 2005; Amorosi *et al.*, 2019); (iii) a robust sequence-stratigraphic framework (Amorosi *et al.*, 2017; Bruno *et al.*, 2017) and (iv) availability of well-dated successions (Campo *et al.*, 2017; Fig. 1).

A specific objective of this study was to assess the environmental drivers that controlled the spatial and temporal distribution of coastal palaeocommunities along a depositional profile (i.e. along-dip) during the Holocene RSL cycle (i.e. marine transgression + sea level highstand; Vacchi *et al.*, 2016), meanwhile allowing a better understanding of landscape dynamics at a millennial timescale.

Study site

Geomorphological setting

The Po delta–coastal plain is a broad area (about 3500 km^2) that mostly lies below mean sea level (Correggiari *et al.*, 2005). It is bounded by the Adige Delta and the Venice Lagoon to the north, and the Northern Apennines dramatically reduce the extension of the plain to the south. This flat area includes the modern delta, mainly formed after a major avulsion (Rotta di Ficarolo) dated to ~800 a BP, and a triangle-shaped plain that develops along the palaeo-Po river course, downstream of the city of Ferrara, where the minimum gradient is reached (Fig. 1). The modern delta is a wave-dominated system that recently evolved towards a more cuspate morphology (Correggiari *et al.*, 2005) under the North Adriatic microtidal regime (tidal currents currently <1 m; Sedrati *et al.*, 2011).

Abandoned or regulated channels (e.g. Po di Volano, Po di Primaro; Fig. 1) occur across the southern plain from west to east. A set of straight to arcuate beach ridges dated back to pre-Etruscan times through archaeological data (Bondesan *et al.*, 1995; Regione Emilia-Romagna, 1999) mark the development of late Holocene shallow-marine sediments in the eastern sector of the coastal plain. South of the modern delta and behind the sand ridges, a large humid area hundreds of square kilometres wide typified by Holocene palustrine and back-barrier wetland deposits occurs (Fig. 1). This area was partly reclaimed through drainage in the second part of the last century for agriculture activities (Cremonini *et al.*, 2008).

Holocene stratigraphy

A transgressive–regressive sedimentary wedge, ~30 m thick, makes up the Holocene succession of the Po delta–coastal plain. Its lower boundary is generally marked by a weakly developed palaeosol
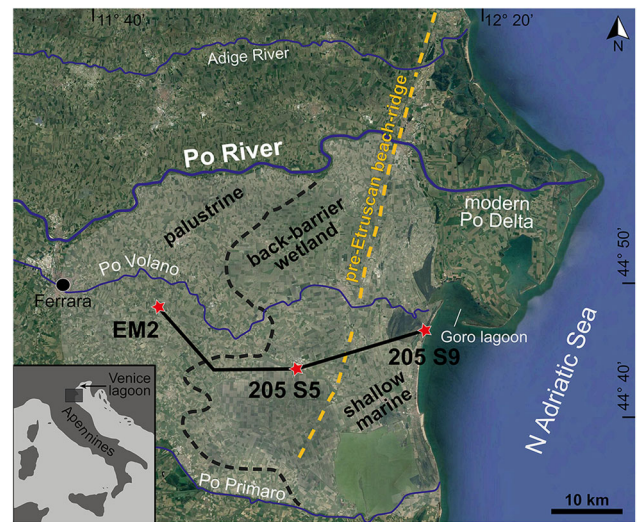
Figure 1. Location map of the study area. The southern portion of the Po coastal-delta plain and its main (palaeo)river branches are highlighted, along with the position of the studied cores (red stars) and the section trace of Fig. 2 (black line). The dotted orange line shows the innermost outcropping beach-ridge. The palustrine, back-barrier wetland and shallow marine sectors correspond to those discussed in the text and identified on the basis of the Holocene stratigraphy. The basemap is a satellite imagery provided by Google Earth. [Color figure can be viewed at wileyonlinelibrary.com]

physically coincident with the Transgressive Surface (Amorosi *et al.*, 2016, 2017; Campo *et al.*, 2020; Fig. 2). A retrogradational pattern of poorly drained floodplain–paludal–lagoon–shallow-marine deposits testifies of the landward migration of an early Holocene estuarine system under the combined action of high rates of RSL rise and climate amelioration (Fig. 2; Bruno *et al.*, 2017; Cacciari *et al.*, 2020).

Complex trends in delta growth and coastal progradation occurred in response to the RSL stabilization between ~7.7 and 7.0k cal a BP (Amorosi *et al.*, 2019). First, bay-head delta progradation took place within the Po estuary, followed by the development of shallow, wave-dominated deltas that shifted along the coastline between ~7.0 and 2.0k cal a BP [lower HST (highstand systems tract); net progradation of ~2.5 m a^{-1}]. During the last 2000 years (upper HST), river-dominated delta lobes rapidly accumulated in deeper waters (~30 m) documenting a marked increase in sediment supply (net progradation of ~15 m a^{-1}; Amorosi *et al.*, 2019).

At higher resolution, eight millennial-scale parasequences of either autogenic (e.g. delta lobe switching, subsidence changes) or allogenic (RSL and climate variability) origin have been identified within the Holocene coastal wedge. Each parasequence is bounded by a flooding surface highlighted by subtle variations in malacofauna and/or meiofauna content (Amorosi *et al.*, 2017).

Materials and methods

To identify Holocene alternative ecosystem states and associated forcings, the palaeobiological content of three reference cores was investigated along a 35-km-long, sea–land transect (205 S9; 205 S5 and EM2 in Figs. 1 and 2) through stratigraphically based, multivariate analysis.

The robust stratigraphic framework available was used to identify core locations diagnostic of the three main sectors of the system: shallow marine – back-barrier wetland – palustrine (Figs. 1 and 2).
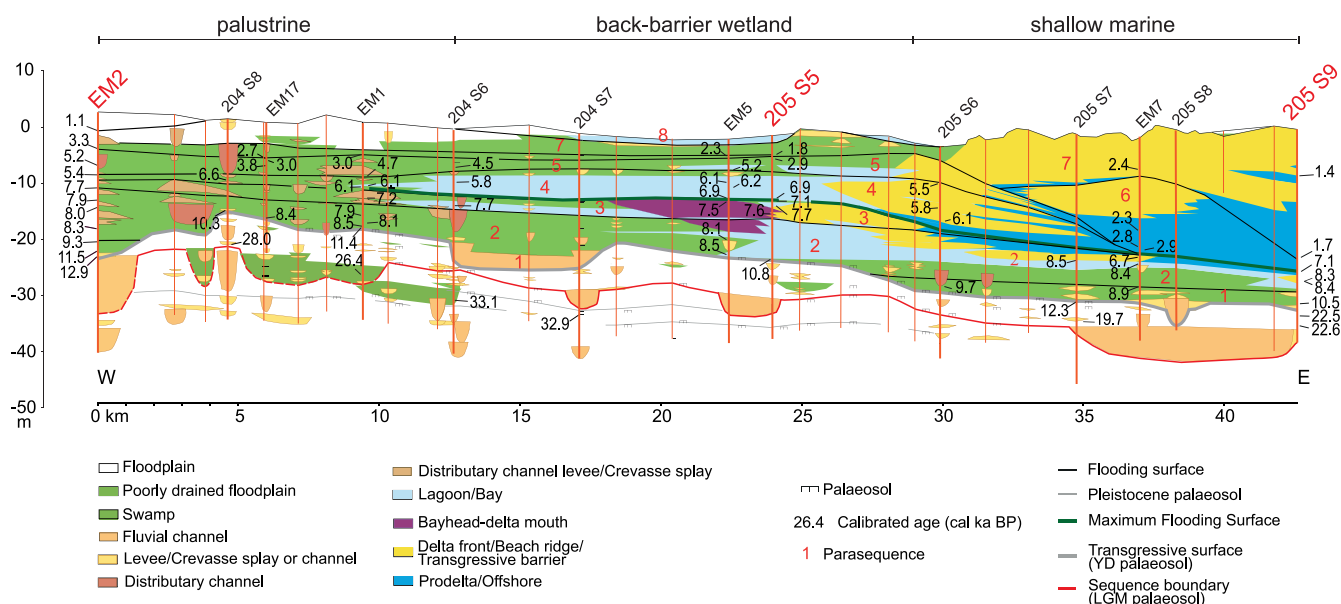
Figure 2. Stratigraphic cross-section, slightly modified from Bruno *et al.* (2017), depicting the Holocene depositional architecture of the study area. Studied cores are highlighted in red and radiocarbon ages are reported as cal a BP. [Color figure can be viewed at wileyonlinelibrary.com]

Core data

The three cores, ~35–40 m long, were recovered by a continuous perforating system that guaranteed an undisturbed stratigraphy and a high recovery percentage (>90%). The sedimentological characterization of the cored successions has been reported in previous works (Amorosi *et al.*, 2003; Bruno *et al.*, 2017; Cacciari *et al.*, 2020). Each core includes a 20–30-m thick Holocene succession predominantly composed of fine-grained deposits (Fig. 2) containing abundant microfossils.

Core 205 S9 [44°46′42″N, 12°15′6″E; 0.30 m below sea level (b.s.l.)] was recovered on an outcropping beach ridge dating back to the Middle Ages (ca. 13th century; Ciabatti, 1967), about 3 km south of the Po di Volano mouth (Fig. 1). Samples from marine deposits, including abundant and well-preserved fossils, were selected for this study (40 samples for benthic foraminifer analysis and 21 for ostracods). The distribution of the main foraminiferal taxa have been recently published in Dasgupta *et al.* (2020). Seven radiocarbon ages are available from this core (Amorosi *et al.*, 2003; Scarponi *et al.*, 2013; Campo *et al.*, 2017).

Core 205 S5 (44°43′38″N, 12°01′40″E; 1.5 m b.s.l.) was recovered ~18 km landward of core 205 S9, in the middle of the back-barrier wetland sector (Fig. 1). Fifty samples were analysed for foraminifers and 42 for ostracods. Ten radiocarbon samples are available for the Holocene succession (Amorosi *et al.*, 2017; Bruno *et al.*, 2017).

Core EM2 [44°48′28″N, 11°47′2.5″E; 2.7 m above sea level (a.s.l.)] was recovered ~18 km inland from 205 S5, within the palustrine sector (Fig. 1). Thirty-six samples were collected for palynological analysis (i.e. pollen and spores). Raw data, pollen zones and associated palaeoclimate implications have been discussed in Cacciari *et al.* (2020). Three additional samples were analysed. Thirteen radiocarbon samples are available from the cored succession (Cacciari *et al.*, 2020).

Palaeobiological data

Samples of approximately 120–100 g were treated adopting the standard methodology described in Amorosi *et al.* (2014) for meiofaunal analysis. The >125-μm size fraction, split into smaller portions, was quantitatively analysed. When possible, at least 300 specimens of benthic foraminifers and 100 valves of ostracods (carapaces were considered as two valves) were counted. Only shells and valves with morphological features sufficiently developed to allow a species-level classification were counted. References for taxonomic identification and ecological interpretation are reported in Table S1. Raw data (number of counted fossils, species, genera and groups) and counts are reported in Tables 1 and S1, respectively.

Palynological samples were prepared following a standard extraction technique (Lowe *et al.*, 1996). Detailed description of the procedure adopted for pollen and spores identification and counting is reported in Cacciari *et al.* (2020). References for taxonomic identification and ecological characterization are shown in Table S1. The structure of the raw dataset is reported in Tables 1 and S1.

Statistical analysis

To streamline the data, all matrices were culled by removing small samples and rare taxa. The minimum threshold value of 300 tests was set for benthic foraminiferal assemblages, and at 20 valves for ostracods (Buzas, 1990; Cronin *et al.*, 1999). To boost palaeoecological information in accordance with microfossil assemblage structure, *ad-hoc* cut-off values and data transformations were applied. The minimum threshold for retained benthic foraminifer and ostracod taxa was set at ≥4% in the marine sector (core 205 S9) and ≥2% in the wetland portion (core 205 S5), following Slack *et al.* (2000). As for pollen in the inland zone (core EM2), a pre-selection was performed. To enhance the local ecological signal, montane taxa and herbs devoid of any specific ecological characterization were excluded from the final matrix. The former belong to the regional pollen rain, as they apparently did not colonize the Po coastal plain during the Holocene (Accorsi *et al.*, 1999, 2004; Cacciari *et al.*, 2020). Then, we retained agglomerated taxa (referred to as 'taxa' from here onwards) with a relative abundance ≥2% in more than one sample. Characteristics and abundances of the final matrices are reported in Tables 1 and S2. Concerning data transformation, we applied the Hellinger transformation in the marine portion, as it downweights the contribution of rare taxa and efficiently models ecological changes, even within short environmental gradients (Legendre and Gallagher, 2001; Legendre and De Cáceres, 2013). The fourth-root transformation was applied in

Table 1. Main characteristics of the raw data matrix and final data matrix used for statistical analyses (CA and DCA) of cores 205 S9 (shallow-marine sector), 205 S5 (back-barrier wetland sector) and EM 2 (palustrine sector). As several grains could not be determined beyond the genus or the family level, the generic word 'taxa' was preferred for palynomorphs. For the final data matrix, the 30 agglomerated taxa used for statistical analysis are sums of species belonging to the same genus (e.g. *Quercus* dec. includes *Q. cerris*, *Q. pubescens*, *Q. robur* and *Quercus* sp.) or genera and species belonging to the same family (e.g. Nymphaeaceae includes *Nymphaea alba*, *Nuphar lutea* and Nymphaeaceae undiff.), if sharing the same ecological features. For cores location and stratigraphy, see Figs. 1–3.

Core	Fossil group	Raw data matrix	Final data matrix
205 S9	Benthic foraminifers	14 545 specimens 31 genera 73 species 2 groups	13 411 specimens 12 genera 10 species 5 groups
	Ostracods	1492 valves 27 genera 41 species 2 groups	1440 valves 15 genera 14 species 4 groups
205 S5	Benthic foraminifers	9643 specimens 19 genera 17 species 1 group	9293 specimens 8 genera 6 species 4 groups
	Ostracods	1641 valves 14 genera 24 species	1586 valves 12 genera 11 species
EM2	Palynomorphs (pollen and spores)	12 136 grains 187 taxa	10 127 grains 90 taxa 30 agglomerated taxa

the transitional portion, as it drastically reduces the contribution of the dominant taxa and increases the statistical weight of low-abundance taxa (Jongman *et al.*, 1995; Magurran, 2004). As for pollen, total abundances were converted into relative frequencies for each sample.

To highlight palaeocommunities composition and structure, R-mode cluster analysis (CA) was separately performed on each microfossil group using the unweighted pair-group method with arithmetic averaging (UPGMA). We used the Horn's modified version of Morisita as a similarity index for benthic foraminifers and ostracods, which is considered one of the most effective measures of similarity for quantitative data (Magurran, 2004 and references therein). Correlation was used as a similarity measure for palynological data, as it proved to be powerful in facies-heterogeneous contexts (e.g. Kaniewski *et al.*, 2013, 2016). Detrended correspondence analysis (DCA) was also applied to investigate palaeobiological turnover and the main controlling driver(s) in distinct, but adjacent depositional settings of the plain. This unconstrained ordination approach has proved to be effective in identifying major palaeoecological changes within stratigraphic records (e.g. Gliozzi and Grossi, 2008; Pascual *et al.*, 2008; Belanger and Garcia, 2014; Correa Metrio *et al.*, 2014; Laut *et al.*, 2016; Rossi *et al.*, 2018; Azzarone *et al.*, 2020). To support the identification of environmental–ecological shifts along each cored succession, we performed a stratigraphically constrained cluster analysis (CONISS; Grimm, 1987) using the same distance matrices adopted in the R-mode clustering and a broken stick model to identify a significant number of groups

(Bennett, 1996). Statistical analyses were performed in the R environment (R 3.6.1; R Core Team, 2019) using the packages 'vegan' (Oksanen *et al.*, 2019), 'factoextra' (Kassambara and Mundt, 2020) and 'rioja' (Juggins, 2020).

Age–depth model

We constructed an age–depth model for each cored succession by using ^{14}C accelerator mass spectrometry (AMS) dates obtained from wood/plant fragments, peat, organic-rich clays or shell samples (Table 2). One date (4500 ± 40; Table 2) from the nearby core EM S5 (Fig. 2) was included to further constrain the model for the upper portion of 205 S5. All dates were calibrated by utilizing the IntCal 13 or the Marine 13 curves, and a mixed curve with 50% of marine component was selected for brackish samples (Reimer *et al.*, 2013). To compensate for the reservoir effect, mollusc samples were calibrated using an average DeltaR value of 139 ± 28 estimated for the northern Adriatic Sea (Langone *et al.*, 1996).

Bayesian age–depth models were developed using the 'rbacon' package version 2.4.2 (Blaauw and Christen, 2011) in the R environment. Several million Markov chain Monte Carlo iterations were applied to generate weighted mean age estimates with 95% confidence intervals (Blaauw and Christen, 2011) at 5-cm intervals along the cores. Prior information, such as changes in accumulation rates, was supplied to refine the models in accordance with core stratigraphy (further details are reported in Appendix S1).

Results

Chronology

Thirty-one AMS ^{14}C dates (Table 2) provide the baseline to reconstruct the chronological framework against which bio-sedimentary changes can be plotted and interpreted. Calibrated ages consistently indicate that the studied successions almost completely cover the Holocene period (Fig. 3).

Although ^{14}C dating can be problematic in coastal and shallow marine–deltaic deposits due to reworking, bioturbation and/or taphonomic processes (Stanley and Chen, 2000; Scarponi *et al.*, 2017), most radiocarbon dates are stratigraphically coherent, with only a few exceptions (Table 2). Despite contrasting resolution of the different age–depth plots (Fig. 3), changes in accumulation rates allow the identification of two chronostratigraphic intervals (i.e. ~11 000–7000/6000 and <7000/6000 cal a BP) that reflect distinct patterns of sediment flux and storage along the depositional profile.

The oldest interval, which encompasses the early Holocene up to ~7000/6000 cal a BP, denotes a progressive increase in accumulation rates within the palustrine and back-barrier sectors with a distinct step around 8500 cal a BP (from 0.12 to 0.6 cm a^{-1} in core EM2 and from 0.14 to 0.4 cm a^{-1} in core 205 S5; Fig. 3B, C). An opposite trend is recorded basinward, as the estimated rate slightly decreases (Fig. 3A). From 7000/6000 cal a BP onwards, a marked decrease in accumulation rates occurs in the palustrine and back-barrier areas (mean value of ~0.14–0.16 cm a^{-1}; Fig. 3B, C), with minor oscillations. Highly variable accumulation rates characterize the shallow-marine sector. A long period of very low sediment storage (estimated rate of ~0.06 cm a^{-1}) is recorded between 7000/6000 and 1700 cal a BP, with no stratigraphic discontinuity associated (Amorosi *et al.*, 2003). Mollusc data from core 205 S9 (Scarponi and Angeletti, 2008; Scarponi *et al.*, 2013) support the hypothesis of a condensed section deprived of significant hiatus. Since 1700 cal a BP, a rapid increase in net accumulation rates occurred (~3 cm a^{-1}; Fig. 3A).

Table 2. AMS ^{14}C dating results reported in this paper.

| Core sample depth (m)	Dating material	Conventional age (a BP)	Calibrated age (2σ cal a BP)	Age–depth model	References
205 S9_35.3	Wood fragments	18 830 ± 140	23 035–22 410	Not included	Amorosi et al. (2003)
205 S9_31.2	Plant fragments	9500 ± 80	11 110–10 570	Included	Amorosi et al. (2003)
205 S9_26.95	Shells/Varicorbula	8075 ± 30	8501–8316	Included	Scarponi et al. (2013)
205 S9_26.95	Shells/Lentidium	7975 ± 30	8382–8192	Included	Scarponi et al. (2013)
205 S9_25.3	Shell	6440 ± 50	7225–6950	Included	Campo et al. (2017)
205 S9_22.4	Shell	2000 ± 40	1800–1570	Included	Campo et al. (2017)
205 S9_8.4	Organic clay	2013 ± 57	1560–1285	Included	Amorosi et al. (2003)
205 S5_22.4	Wood fragments	9445 ± 85	10 905–10 490	Included	Amorosi et al. (2017)
205 S5_19.35	Shell	7990 ± 50	8640–8415	Included	This study
205 S5_17.7	Shell	7940 ± 50	8590–8400	Included	This study
205 S5_14	Wood fragments	6690 ± 50	7655–7475	Included	Bruno et al. (2017)
205 S5_12.7	Wood fragments	6860 ± 50	7795–7590	Included	Amorosi et al. (2017)
205 S5_11.65	Wood fragments	6190 ± 40	7180–6975	Included	Amorosi et al. (2017)
205 S5_11.25	Wood fragments	6260 ± 50	7275–7140	Included	Amorosi et al. (2017)
205 S5_8.65	Wood fragments	6150 ± 50	7170–6900	Included	This study
EM5_6.9	Wood fragments	4500 ± 40	5305–5040	Included	Amorosi et al. (2017)
205 S5_4.2	Wood fragments	2750 ± 40	2930–2765	Included	Amorosi et al. (2017)
205 S5_3.35	Wood fragments	1890 ± 40	1900–1720	Included	Amorosi et al. (2017)
EM2_25.45	Plant fragments	11 110 ± 50	13 065–12 820	Not included	Cacciari et al. (2020)
EM2_24.5	Plant fragments	9990 ± 50	11 650–11 260	Included	Cacciari et al. (2020)
EM2_22.90	Wood fragments	8320 ± 50	9470–9200	Included	Cacciari et al. (2020)
EM2_20.55	Wood fragments	7470 ± 50	8380–8185	Included	Cacciari et al. (2020)
EM2_16.6	Wood fragments	7140 ± 40	8025–7925	Included	Cacciari et al. (2020)
EM2_15.3	Peat	7070 ± 40	7975–7825	Included	Cacciari et al. (2020)
EM2_15.2	Plant fragments	7460 ± 40	8365–8190	Included	Cacciari et al. (2020)
EM2_14.65	Wood fragments	6630 ± 40	7575–7440	Included	Cacciari et al. (2020)
EM2_13.35	Plant fragments	6840 ± 40	7760–7590	Included	Cacciari et al. (2020)
EM2_11.1	Plant fragments	4680 ± 40	5480–5315	Included	Cacciari et al. (2020)
EM2_9.45	Wood fragments	4480 ± 30	5240–5035	Included	Cacciari et al. (2020)
EM2_6.45	Plant fragments	3110 ± 80	3485–3075	Included	Cacciari et al. (2020)
EM2_3.2	Wood fragments	1180 ± 40	1185–980	Included	Cacciari et al. (2020)
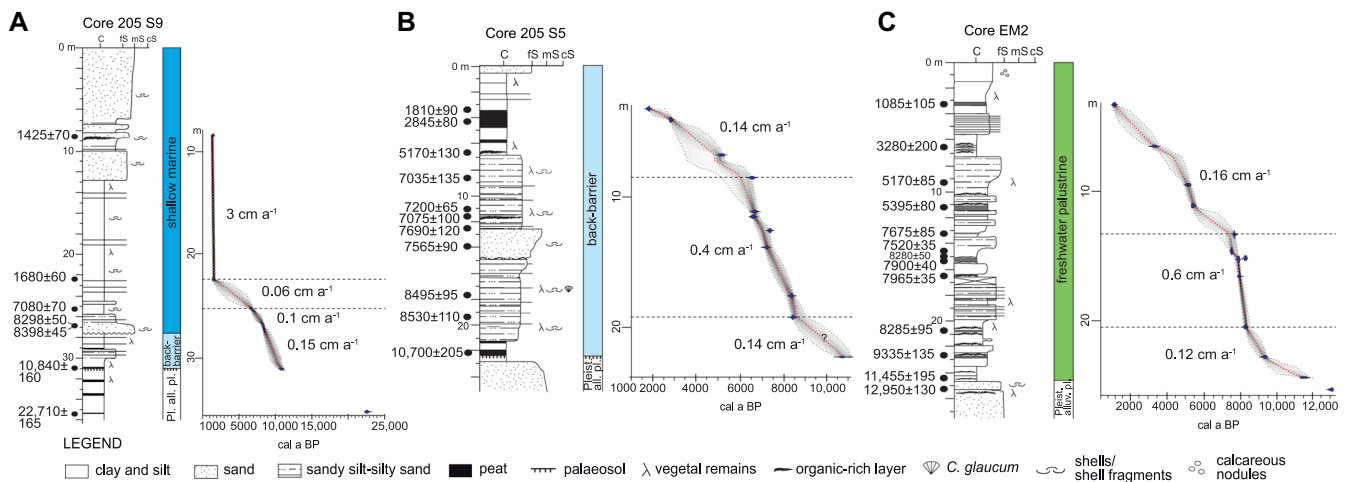
Figure 3. Stratigraphy, depositional environments and the age–depth model of cores 205 S9 (A), 205 S5 (B) and EM2 (C). Age estimates were obtained using the "rbacon" package version 2.4.2 (Blaauw and Christen, 2011) in the R environment (R Core Team, 2019). Dotted grey lines show 95% confidence intervals, while the dotted red line displays the single 'best' model based on the mean age for each depth. Darker greys indicate more likely calendar ages. Black dashed lines highlight the main changes in accumulation rates, calculated as the thickness of the stratigraphic interval divided by the difference between the median calibrated ages. Model parameter settings are reported in Appendix S1. Depositional environments derived from Fig. 2. [Color figure can be viewed at wileyonlinelibrary.com]

Shallow-marine fossil record

Meiofauna composition

A very rich meiofauna composed of abundant benthic foraminifers and ostracods is encountered (Table 1; Table S1). The R-mode CA reveals three clusters (S9 F1–F3) and one singleton (Nonionella turgida–N. stella) for benthic foraminifers and three clusters (S9 O1–O3) for ostracods (Fig. 4A, B; Table 3).

Cluster S9 F1 is composed of several shallow-marine taxa typically thriving on Mediterranean inner shelves (i.e. water depth <40 m) subject to low river inputs (Jorissen, 1988; Frezza and Carboni, 2009). The cluster also includes a set of epiphytic taxa (e.g. Textularia, Rosalina, Elphidium, Triloculina and Adelosina species; Langer, 1993), some of which are very sensitive to riverine organic matter fluxes (Jorissen et al., 2018).
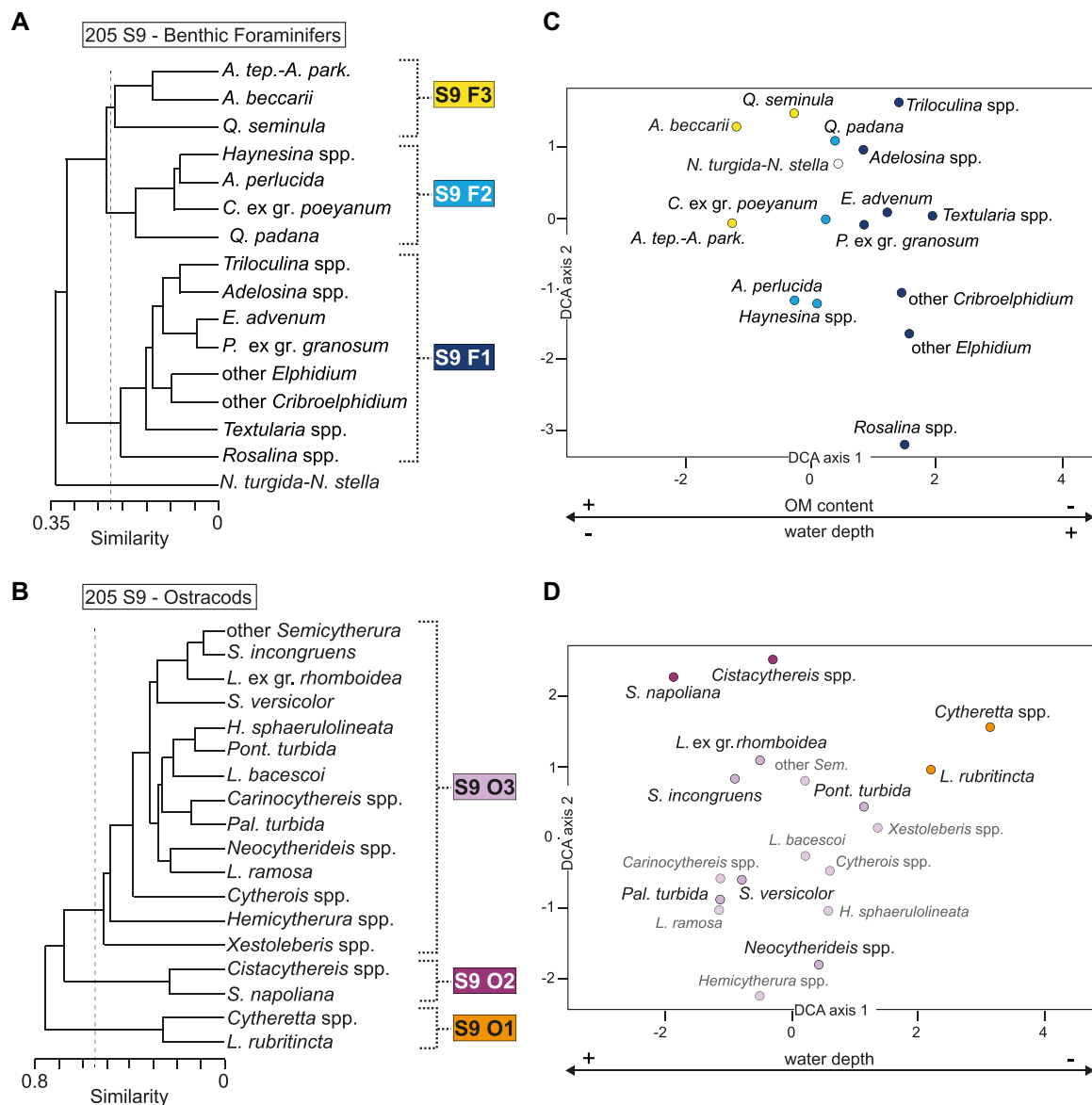
Figure 4. Results of the statistical analysis performed on the meiofauna of core 205 S9 (shallow marine sector – Figs. 1 and 2). (A,B) R-cluster output (UPGMA, Horn's modified version of Morisita index) for benthic foraminifer and ostracod data, respectively. Dotted lines correspond to the cut-off levels. (C,D) DCA output reports for benthic foraminifer (DC1 variance: ~59%; DC2 variance: ~14%) and ostracod (DC1 variance: ~39%; DC2 variance: ~29%) taxa, respectively. Key taxa are shown with solid colours. Each colour corresponds to a specific cluster/singleton. The scale of axis 1 differs in the distinct diagrams. Samples are plotted in Fig. S1 of Appendix S2. [Color figure can be viewed at wileyonlinelibrary.com]

Cluster S9 F2 includes opportunistic foraminifers tolerant to moderate–high fluxes of organic matter (OM) and preferring muddy substrates (e.g. *A. perlucida*, *Haynesina* spp., *Quinqueloculina padana*; Jorissen, 1988; Jorissen *et al.*, 2018). On the North Adriatic shelf, a comparable association of taxa characterizes nutrient-rich, proximal prodelta areas located downdrift of the main delta mouths at water depths between ~10 and 20 m (Donnici and Serandrei Barbero, 2002; Barbieri *et al.*, 2019).

Cluster S9 F3 consists of nearshore species (*Ammonia* species and *Quinqueloculina seminula*) that presently thrive in the North Adriatic coastal belt on mixed substrates (mud–sand) and that contain variable OM amounts (Jorissen, 1988; Donnici and Serandrei Barbero, 2002).

Lastly, the singleton *Nonionella turgida–N. stella* represent mud-dwelling, opportunistic taxa suited to environments rich in organic matter (Van Der Zwaan and Jorissen, 1991; Bernhard *et al.*, 1997).

About ostracods, cluster S9 O1 gathers two nearshore taxa (*Loxoconcha rubritincta* and *Cytheretta* spp.) that prefer sandy bottoms and water depths <20 m in the North Adriatic (Masoli, 1968; Breman, 1975; Tsourou, 2012).

Cluster S9 O2 includes infralittoral–upper circalittoral taxa (*Sagmatocythere napoliana* and *Cistacythereis* spp.) typically recorded on sand–mud substrates (Bonaduce *et al.*, 1975). Cluster S9 O3 includes several infralittoral to infralittoral–upper circalittoral taxa with variable preferences in terms of substrates and OM content (e.g. *Pontocythere turbida*, *Palmoconcha turbida*, *Sagmatocythere versicolor*, *Semicytherura incongruens*).

Indirect gradient analysis

The application of DCA reveals a continuous distribution of both benthic foraminifer and ostracod taxa along the major axis of variation (DCA axis 1 in Fig. 4C, D). This axis underlines a distinct (palaeo)environmental factor(s), whereas the second axis cannot be related to any discernible parameters.

In the benthic foraminifer plot, the turnover expressed along axis 1 (~59.4% of data variance vs. 14.2% explained by DCA axis 2) is interpreted to reflect the degree of fluvial influence, mainly expressed by OM concentration, and water depth (Fig. 4C). Taxa sensitive to organic enrichment and preferring

Table 3. Microfossil clusters and associated ecological–environmental features.

Cluster	Main taxa	Ecological–environmental characteristics
S9 F1	*Rosalina* spp., *Textularia* spp., *Adelosina* spp., *Triloculina* spp.	Inner shelf (i.e. water depth <40 m) with vegetated bottoms, subject to low river inputs (e.g. low turbidity, low OM fluxes)
S9 F2	*Aubignyna perlucida*, *Haynesina* spp., *Quinqueloculina padana*	Inner shelf (i.e. water depth <20 m) subject to high river inputs (e.g. high OM fluxes)
S9 F3	*Ammonia tepida–A. parkinsoniana*, *Ammonia beccarii*	Inner shelf (i.e. water depth <15–20 m) with mixed substrates (mud-sand) and a variable OM amount
S9 O1	*Loxoconcha rubritincta*, *Cytheretta* spp.	Inner shelf (i.e. water depth <15–20 m) with sandy substrates
S9 O2	*Sagmatocythere napoliana*, *Cistacythereis* spp.	Inner-mid shelf with sand–mud substrates
S9 O3	*Pontocythere turbida*, *Palmoconcha turbida*, *Semicytherura incongruens*	Inner shelf (i.e. water depth <40 m) subject to variable river inputs (e.g. OM fluxes)
S5 F1	*Helenina anderseni*, *Trochammina inflata*	Brackish vegetated areas subject to oscillating water levels as salt-marshes
S5 F2	*Ammonia tepida–A. parkinsoniana*, *Haynesina germanica*, *Aubignyna perlucida*, *Porosononion* ex gr. *granosum*	Back-barrier basins with bottoms enriched in OM and variable salinity conditions (e.g. lagoon, estuary, bay)
S5 O1	*Cyprideis torosa*, *Loxoconcha elliptica*, *Cytheromorpha fuscata*, *Leptocythere castanea*, *Pontocythere turbida*	Back-barrier basins with variable salinity conditions and changeable rates of seawater exchange (e.g. lagoon, estuary, bay)
S5 O2	*Pseudocandona* cf. *albicans*, *Metacypris cordata*, *Candona* spp.	Shallow, standing, hypohaline water bodies enriched in vegetation masses as paludal basins
EM2 P1	Callitrichaceae, Poaceae, Pteridophyta, *Sparganium* spp.	Freshwater deep fens with emerged portions, probably located on their fringes
EM2 P2	*Salix*, *Typha* spp., Ranunculaceae, Brassicaceae	Riparian willow woods with associated submerged and dry areas depending on local morphologies
EM2 P3	Asteroideae, Cichorioideae, Chenopodiaceae, Apiaceae, Caryophyllaceae, Urticaceae	Mesophilous grasslands with (mostly) natural pastures and disturbed, nitrophilous areas
EM2 P4	*Tilia*, Cyperaceae, Nympheaceae	Freshwater shallow fen with emerged portions populated by lime trees
EM2 P5	Deciduous *Quercus* spp., *Q. ilex*, *Alnus glutinosa*, *Corylus avellana*	Lowland mixed oak–alder–holm oak forest developed either on well-drained soils (oak woods) or on hygrophilous/partially saturated soils (alder woods)

relatively deep water depths far from river outlets (cluster S9 F1) assemble on the right side of the biplot (DC1 > 0.8). In contrast, indifferent or opportunistic species thriving on moderate to high OM levels at shallow water depths (S9 F2–F3 taxa and the singleton *N. turgida–N. stella*) occur in the centre-left sector (DC1 < 0.4).

As for ostracods, the environmental gradient underlying axis 1 (~39% of data variance vs. 28.7% explained by DCA axis 2) is inferred to be driven mainly by bathymetry (Fig. 4D). Nearshore taxa in cluster S9 O1 occur on the right extremity of the biplot (DC1 > 2), whereas lower positive scores of DCA axis 1 characterize infralittoral taxa of cluster S9 O3 (e.g. *Pont. turbida*, *Neocytherideis* species). Infralittoral–upper circalittoral taxa belonging to clusters S9 O3 (e.g. *S. versicolor*, *S. incongruens*, *Palm. turbida*) and S9 O2 (e.g. *S. napoliana*, *Cistacythereis* spp.) plot on the left portion, showing negative DC1 scores. Although bathymetry is a complex gradient commonly accompanied by variations in substrate granulometry (e.g. Boomer and Eisenhauer, 2002; Barbieri *et al.*, 2019), no significant correlation with sand content can be inferred from the ostracod distribution (Fig. 4D).

Back-barrier fossil record

Meiofauna composition

A rich, well-preserved meiofauna characterizes core 205 S5 (Table 1; Table S1). An exception is represented by the 2.5-m-thick sandy interval recorded between ~12.5 and 15 m core depth (Fig. 3B), which contains few, poorly preserved microfossils considered transported inland by marine currents. The R-mode CA reveals two clusters (S5 F1 and S5 F2) and two singletons (Miliolids and *Cribroelphidium* ex gr. *poeyanum*) for benthic foraminifers and two clusters (S5 O1–O2) and one singleton (*Darwinulina stevensoni*) for ostracods (Fig. 5A, B; Table 3).

Cluster S5 F1 is composed of two euryhaline species: *Helenina anderseni* and *Trochammina inflata*. The former is commonly found within salt marshes and tidal flats (Giordana *et al.*, 2011 and references herein). The latter is an agglutinated foraminifer commonly reported from vegetated high to mid marshes (e.g. Horton and Edwards, 2006; Murray, 2006; Leorri *et al.*, 2008). In the Mediterranean area, the co-occurrence of these species characterizes the Venice Lagoon marshes (Serandrei Barbero *et al.*, 2004).

Cluster S5 F2 consists of several taxa, two of which (*Ammonia tepida–A. parkinsoniana* and *Haynesina germanica*) are euryhaline, opportunistic species thriving in restricted environments characterized by brackish salinity and OM enrichment (Debenay and Guillou, 2002; Murray, 2006). Shallow-marine taxa tolerant to remarkable amounts of OM also belong to cluster S5 F2 (e.g. *Porosononion* ex gr. *granosum* and *A. perlucida*; Jorissen *et al.*, 2018). A comparable foraminiferal assemblage is recorded within several Mediterranean lagoons (e.g. Zampi and D'Onofrio, 1986; Melis and Covelli, 2013; Benito *et al.*, 2016).

The singleton *Cribroelphidium* ex gr. *poeyanum* has been reported behind the sandy spit of the Goro lagoon (modern Po Delta; Fig. 1), where restricted conditions occur (Coccioni, 2000). The other singleton includes the Miliolid group, mainly represented by *Quinqueloculina*, *Miliolinella* and *Pseudotriloculina* species, and is invariably associated with species of cluster S5 F2 (Table S2). In Mediterranean lagoons, diversified assemblages with common Miliolids indicate inlet areas with substantial marine influence and low confinement (Debenay, 2000).

As for ostracods, cluster S5 O1 includes the truly euryhaline *Cyprideis torosa* and a set of brackish–marine taxa (e.g. *Loxoconcha elliptica*, *Leptocythere lagunae*, *Leptocythere bacescoi*, *Cytheromorpha fuscata* and *Xestoleberis* species) typical of estuarine-lagoonal areas (Mazzini *et al.*, 2017 and
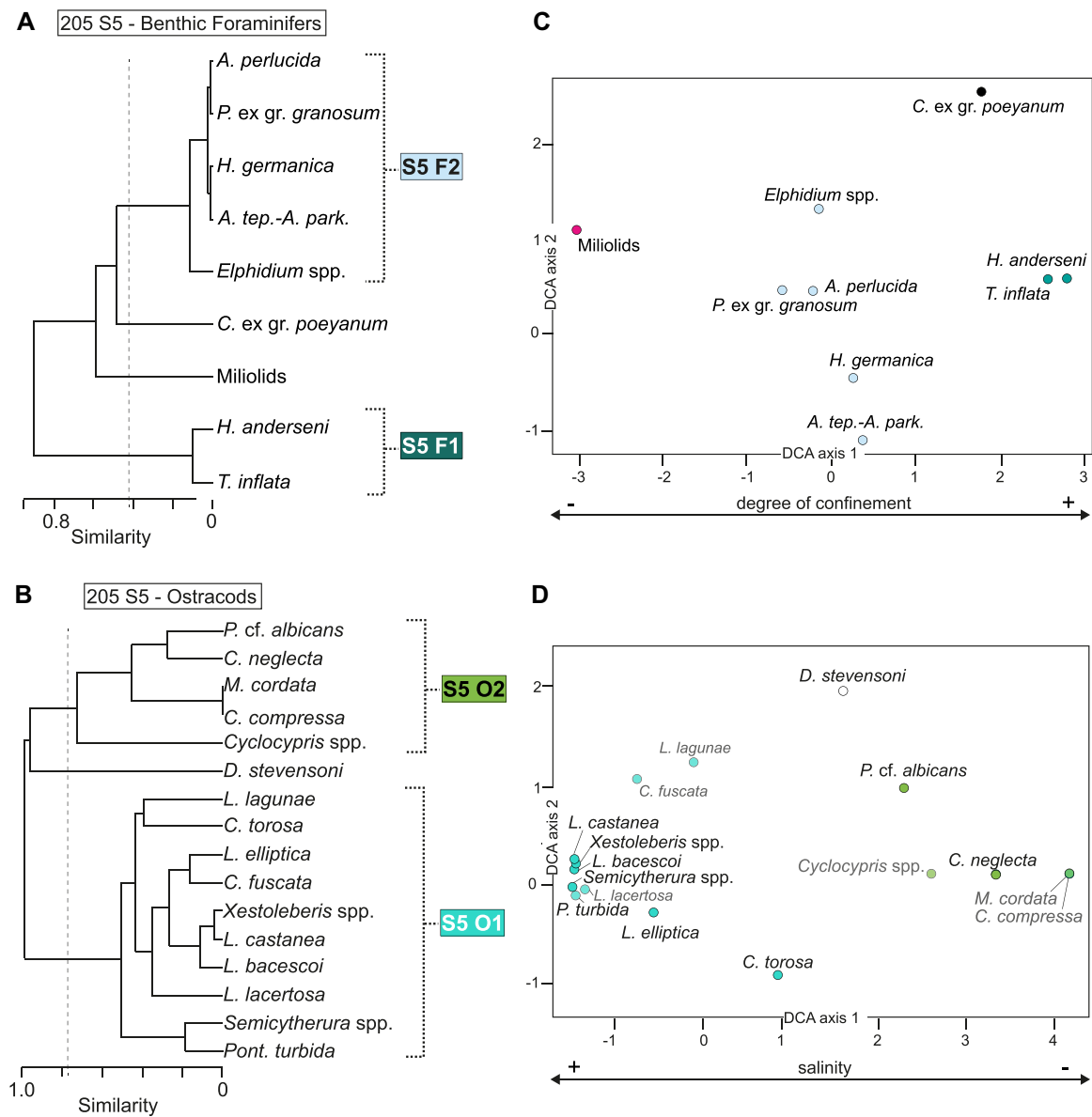
Figure 5. Results of the statistical analysis performed on the meiofauna of core 205 S5 (back-barrier wetland sector – Figs. 1 and 2). (A,B) R-cluster output (UPGMA, Horn's modified version of Morisita index) for benthic foraminifer and ostracod data, respectively. Dotted lines correspond to the cut-off levels. (C,D) DCA output reports for benthic foraminifer (DC1 variance: ~53%; DC2 variance: ~15%) and ostracod (DC1 variance: ~57%; DC2 variance: ~20%) taxa, respectively. Key taxa are shown with solid colours. Each colour corresponds to a specific cluster/singleton. The scale of axis 1 differs in the distinct diagrams. Samples are plotted in Fig. S2 of Appendix S2. [Color figure can be viewed at wileyonlinelibrary.com]

references herein). Nearshore ostracods, such as *Pont. turbida* and *Semicytherura* species also occur. A partial replacement of *C. torosa* by nearshore ostracods is commonly documented in proximity of the inlets and/or under low confinement conditions (e.g. Montenegro and Pugliese, 1996; Ruiz *et al.*, 2000; Salel *et al.*, 2016).

Cluster S5 O2 is composed of freshwater to low brackish ostracods mainly represented by *Pseudocandona* cf. *albicans*, *Candona neglecta* and, less frequently, *Metacypris cordata*. *Pseudocandona albicans* and *M. cordata* prefer shallow, standing water bodies enriched in vegetation masses and can tolerate oxygen deficiency (Meisch, 2000; Frenzel *et al.*, 2010).

The singleton *Darwinula stevensoni* is a mesohaline ostracod preferring slow moving waters and tolerating slightly low oxygen conditions (Meisch, 2000; Frenzel *et al.*, 2010).

Indirect gradient analysis

Taxa distribution along DCA axis 1 documents a well-defined faunal turnover (Fig. 5C, D), which is inferred to be mainly controlled by environmental gradients. DCA axis 2 is not interpretable.

For foraminifers, the strong gradient underlying DCA axis 1 scores (~53% of data variance vs. 15% explained by DCA axis 2) corresponds to the degree of confinement (Fig. 5C), a well-known controlling factor that primarily influences the spatial distribution of benthic assemblages within coastal settings (Debenay and Guillou, 2002; Hayward *et al.*, 2004). Intertidal species of cluster S5 F1 and *C.* ex gr. *poeyanum*, typical of restricted lagoon areas, occupy the far right side of DC1 (scores > 2), while taxa thriving in coastal areas with high rates of seawater exchange (i.e. the singleton Miliolids) plot on the opposite edge (DC1 ~−3). Opportunist taxa (*A. tepida–A. parkinsoniana*, *H. germanica*, *P.* ex gr. *granosum* and *A. perlucida*) able to tolerate salinity oscillations and OM enrichments have intermediate scores (DC1 close to zero) and belong to cluster S5 F2 (Fig. 5C).

The ecology of ostracod species reveals that the ordination pattern along axis 1 (~57.5% of data variance vs. 20% explained by DCA axis 2) is guided by salinity (Fig. 5D), which

is commonly identified as one of the major controlling factors within back-barrier environments (e.g. Laut *et al.*, 2016; Salel *et al.*, 2016; Frenzel, 2019). The position of ostracod taxa follows a positive gradient from right (DC1 positive scores) to left (DC1 negative scores) along the axis of major variation (Fig. 5D). Freshwater to low brackish species, gathered within cluster S5 O2, and the singleton *D. stevensoni* plot on the right extremity of DCA axis 1 (scores > 1). By contrast, marine–brackish (e.g. *L. bacescoi, L. castanea* and *Xestoleberis* species) and marine (e.g. *Pont. turbida* and *Semicytherura* species) ostracods of cluster S5 O1 assemble on the far-left side (DC1 < −1). In the middle portion of DCA axis 1 (between ~1 and −1), brackish species belonging to cluster S5 O1 and able to tolerate ample salinity variations occur (e.g. *L. elliptica* and *C. torosa*).

Palustrine fossil record

Vegetation composition

A high floristic richness typifies the palustrine succession (Table S1). R-mode CA reveals five clusters (EM2 P1–P5; Fig. 6A; Table 3) corresponding to distinct local vegetation communities.

Cluster P1 exclusively includes wetland herbs: some thrive in humid environments (e.g. pteridophytes), some tolerate rather long periods of radical drowning (e.g. *Sparganium erectum*), others live in water, floating or immersed, such as as Callitrichaceae and *Sparganium emersum*. The presence of Poaceae, which exploit a wide variety of environments, suggests the occurrence in this family of hygro-helophytes, commonly found on the fringes of flooded areas, and of pioneer taxa colonizing woodland clearances between woods and swamps. Cluster P2 is characterized by *Salix* along with helophyte *Typha* and other herbs, such as Ranunculaceae and Brassicaceae. The former group includes several wetland and mesophilous species, while the latter includes rather ubiquitous, mesophilous

taxa. This willow wood community is commonly widespread along the riverbanks.

Several meso-xerophilous herbs compose cluster P3. Some of them are typical of pasture grasslands (e.g. Asteroideae and Cichorioideae) or can be related to cultivation (e.g. *Beta vulgaris*), but many others are ubiquitous (e.g. Apiaceae) or pioneering herbs exploiting disturbed environments (e.g. Urticaceae). This cluster reflects the typical disturbed grassland of emerged floodplains, induced by either human presence or natural environmental variability.

Cluster P4 includes hygrophytes (mainly Cyperaceae), aquatics (Nympheaceae) and a mesophilous tree (*Tilia*) tolerant to low degrees of soil humidity. Such a mixed community points to marginal and/or small paludal settings typically formed within partially submerged, freshwater lowlands.

Taxa forming cluster P5 account for a lowland mixed oak woodland (e.g. deciduous *Quercus, Q. ilex, Carpinus*), defined as the Potential Natural Vegetation of the Po Plain (Blasi *et al.*, 2014). The occurrence of *Alnus glutinosa* (swamp forest tree) and *Isoetes* sp. (aquatic fern) indicates the widespread presence of humid environments in the plain, patchily alternating with the mixed oak forest, depending on soil drainage.

Indirect gradient analysis

The first DCA axis explains ~37% of the data variance, whereas axis 2 accounts for ~32%, highlighting the absence of a predominant controlling factor on data ordination, consistent with the high sensitivity of vegetation to a range of parameters. Axis 2 cannot be interpreted as it probably reflects the complex interaction of various environmental factors, including water-table level, soil composition and temperature, among others.

The highest DCA axis 1 scores (>1) are associated with the retrieved ubiquitous and meso-xerophilous herbs
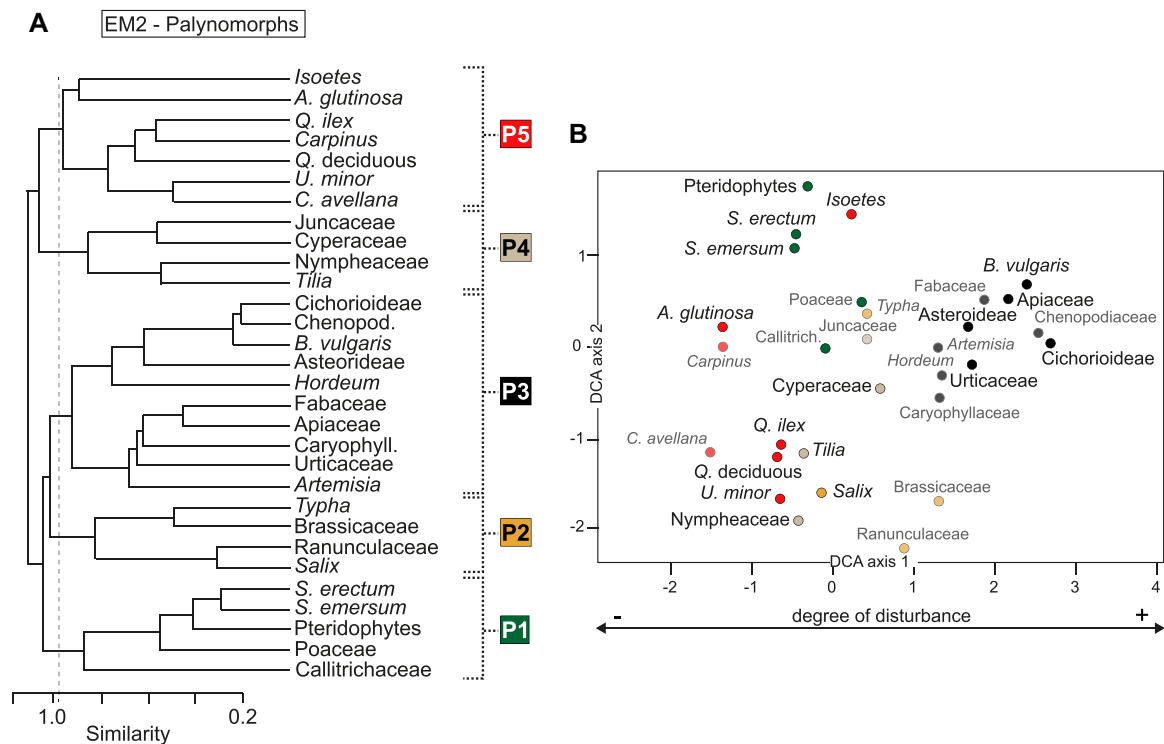
Figure 6. Results of the statistical analysis performed on the meiofauna of core EM2 (palustrine sector – Figs. 1 and 2). (A) R-cluster output (UPGMA, correlation index) for pollen data. Dotted line corresponds to the cut-off level. (B) DCA output report for pollen taxa (DC1 variance: ~37%; DC2 variance: ~32%); key taxa are shown with solid colours. Each colour corresponds to a specific cluster. Samples are plotted in Fig. S3 of Appendix S2. [Color figure can be viewed at wileyonlinelibrary.com]

composing cluster P3. All meso-xerophilous trees (e.g. deciduous *Quercus*, *Q. ilex*, *Ulmus minor*) and hygrophilous *A. glutinosa*, gathered within cluster P5, occur at the opposite edge (DC1 < −0.5) (Fig. 6B). The middle portion of the biplot (DC1 scores between ~−0.5 and 1) includes hygrophytes (e.g. pteridophytes and Cyperaceae) and aquatic herbs (e.g. *Sparganium* sp., *Isoetes* and Nympheaceae), mainly belonging to clusters P1 and P4. Interestingly, two trees (*Salix* and *Tilia*) typifying clusters P2 and P4 show DCA axis 1 scores close to zero.

As a whole, the continuous distribution of taxa along axis 1 may be interpreted as a disturbance gradient from a forested and barely perturbed environment (highly negative scores) to an open landscape firstly dominated by hygro-helo-hydrophytes (scores around zero) and then by pasture-meadow and ubiquitous herbs (highly positive scores). Considering the depositional setting, taxa with intermediate DCA axis 1 scores reasonably represent the vegetation community typical of freshwater paludal areas that can turn into mesophilous woodlands or grasslands if drier topsoil conditions occur.

Discussion

Holocene variability of microtidal ecosystems

If plotted stratigraphically and combined with sedimentological features, palaeobiological results (i.e. R-mode clusters and DC1 sample scores) allow identifying millennial-scale, Holocene environmental–ecological dynamics from the different coastal sectors (Figs. 7–9). These stratigraphic shifts are confirmed by the CONISS results, reported in Appendix S3.

Shallow-marine area

Marine ingression at the study site is recorded around 8700 cal a BP by the abrupt superposition of transgressive barrier sands on a back-barrier succession (Bruno *et al.*, 2017; Figs. 2 and 3). Barrier sands and the overlying 4-m-thick silt–clay succession (up to 22.5 m core depth) contain an infralittoral–upper circalittoral palaeocommunity mainly represented by taxa composing clusters F1 (34–57%) and O3 (>85%), with the secondary occurrence of F2 (20–45%) and O2 (<10%) taxa (Fig. 7). These bio-sedimentological features record the establishment and long-term persistence (up to ~1750 cal a BP) of an open-shelf ecosystem, characterized by a vegetated bottom (abundance of epiphytic taxa in F1), low degree of fluvial influence (low OM concentration, Fig. 7) and scarce sediment input (low sedimentation rate, Fig. 3A). Although rather stable environmental–ecological conditions characterize this interval, two minor shifts occurred around 8000 and 7500 cal a BP (Fig. 7). The older reflects (i) a slight increase in bathymetry, as documented by the increment of cluster O2, and (ii) increasing distance from the river mouth, as documented by the increment of cluster F1, consistent with the lowest OM content encountered within the whole succession (Fig. 7). The younger shift, mainly highlighted by a minor increase in opportunistic foraminifers (cluster F2 Fig. 7; Table 3), tracks an OM turning point (i.e. faint OM enrichment) reasonably linked to an increment of fluvial input to the shelf.

The main ecosystem turnover occurred long after, around 1750 cal a BP (Fig. 7), with the disappearance of infralittoral–upper circalittoral ostracods (cluster O2) and a marked change in the foraminiferal palaeocommunity structure, which displays the substantial replacement of epiphytic taxa by nearshore species thriving in shallow-marine environments subject to variable OM fluxes (cluster F3 > 40%; Table 3). High and unsteady OM inputs are also suggested
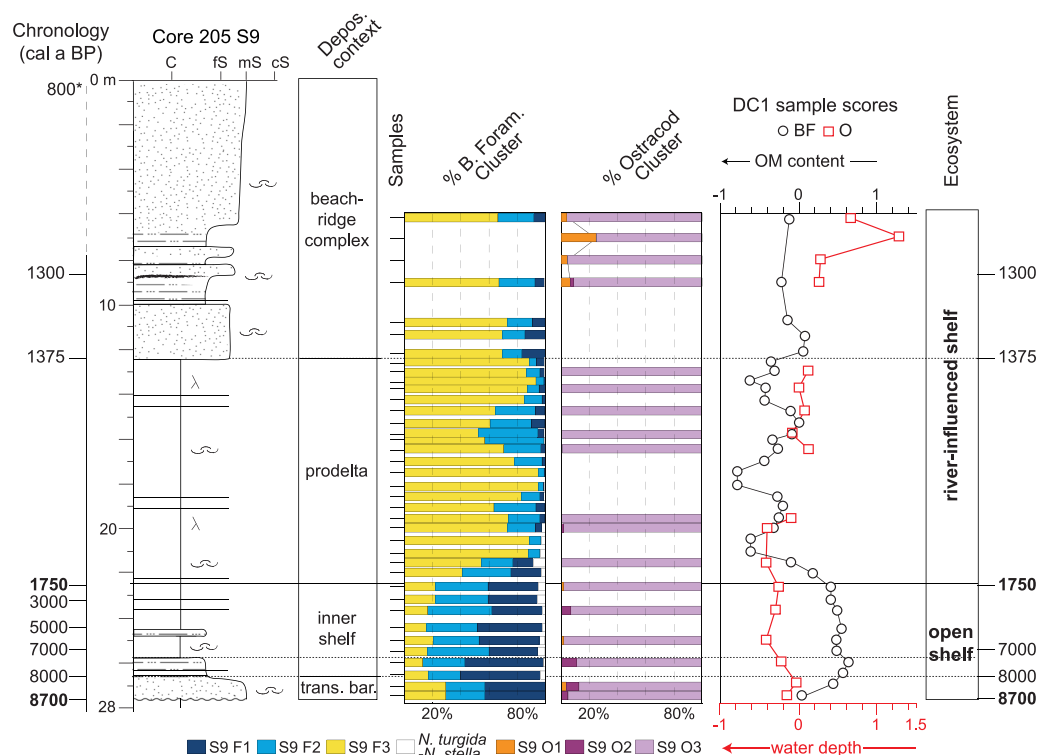
Figure 7. Holocene depositional stacking patterns, ecosystem variability and meiofauna trends across the shallow-marine succession of core 205 S9. Core chronology and lithology are derived from Fig. 3A. Stratigraphic changes in faunal composition (benthic foraminifers and ostracods) are highlighted by the relative abundances of clusters and DC1 sample score trends; the arrow pointing in the direction of DC1 axis indicates an increasing trend of the estimated parameters (OM content, water depth). The age atop the cored succession and highlighted by an asterisk (800* a BP) derives from archaeological data (Ciabatti, 1967). [Color figure can be viewed at wileyonlinelibrary.com]
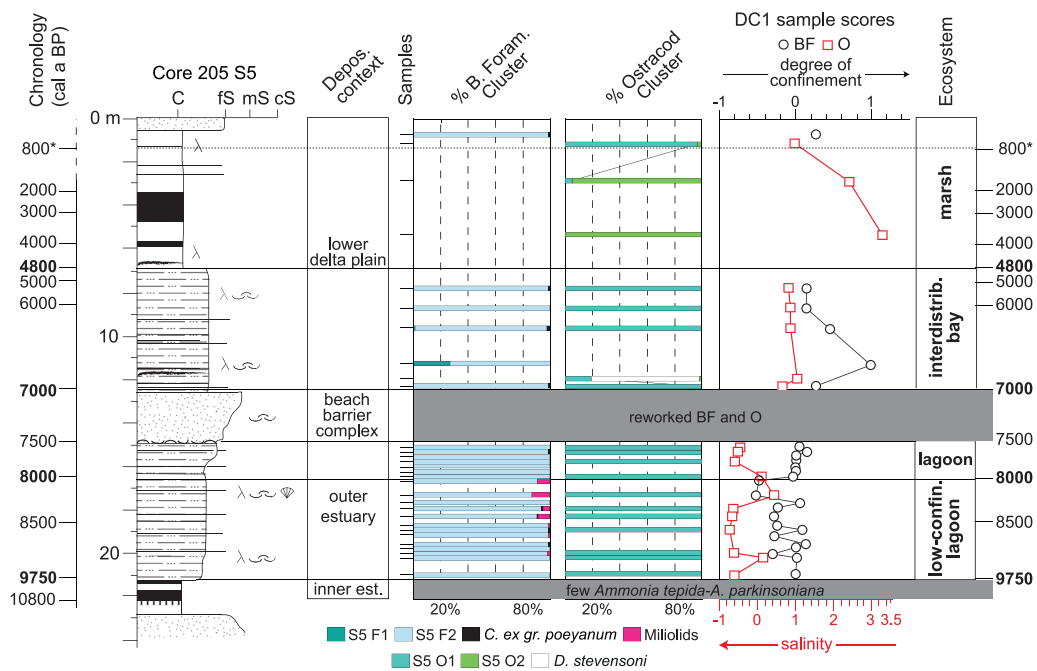
Figure 8. Holocene depositional stacking patterns, ecosystem variability and meiofauna trends across the back-barrier succession of core 205 S5. Core chronology and lithology are derived from Fig. 3B. Stratigraphic changes in faunal composition (benthic foraminifers and ostracods) are highlighted by the relative abundances of clusters and DC1 sample scores trends; the arrow pointing in the direction of DC1 axis indicates an increasing trend of the estimated parameters (degree of confinement, salinity). The DC1 axis scales of BF and O samples are different. The age atop the cored succession and highlighted by an asterisk (800* cal a BP) is from Amorosi *et al.* (2017). [Color figure can be viewed at wileyonlinelibrary.com]
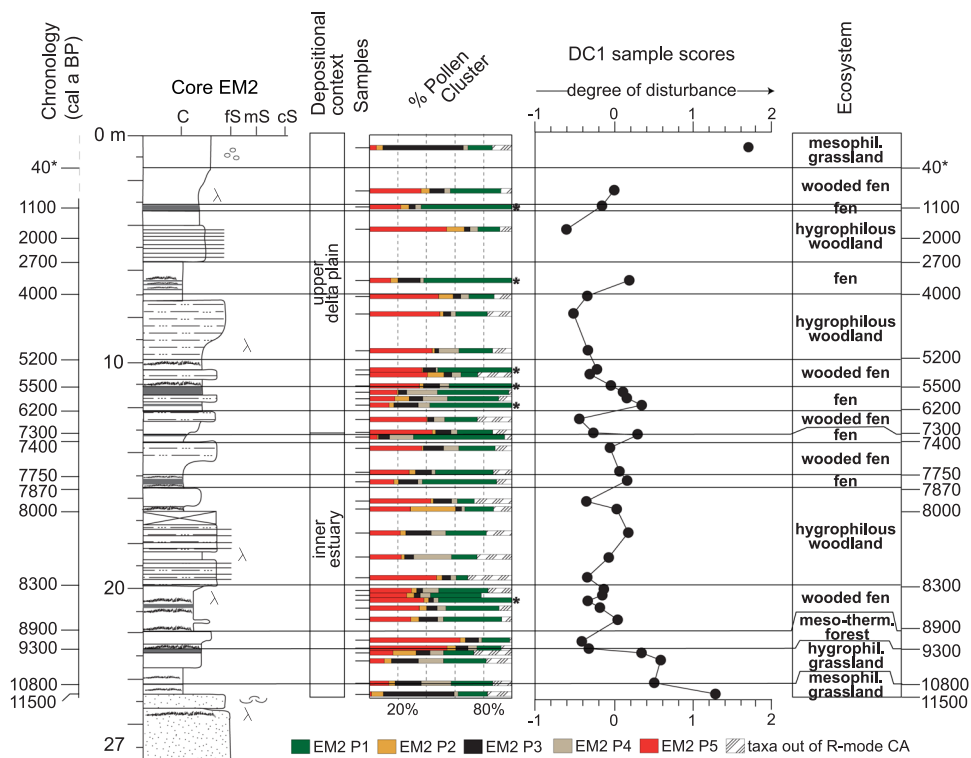
Figure 9. Holocene depositional stacking patterns, ecosystem variability and vegetation trends across the palustrine succession of core EM2. Core chronology and lithology are derived from Fig. 3C. Stratigraphic changes in palynological content are highlighted by the relative abundances of clusters and DC1 sample score trends; the arrow pointing in the direction of DC1 axis indicates an increasing trend of the estimated parameter (degree of disturbance). Asterisks correspond to samples exceeding 100% due to the high abundance (commonly > 20%; Table S2) of pteridophytes; in these samples taxa out of R-mode CA are not plotted. The age atop the cored succession and highlighted by an asterisk (40* a BP) was estimated applying the accumulation rate obtained for the youngest interval of the age depth model (0.16 cm a^{-1}; Fig. 3). [Color figure can be viewed at wileyonlinelibrary.com]

by fluctuating DC1 scores, pointing to a river-influenced shelf ecosystem subject to high sediment fluxes (Figs. 3A and 7). Consistently, an upward decrease in water depth is depicted by the positive shift of DC1 ostracod scores peaking within

beach-ridge sands younger than 1375 cal a BP (Fig. 7). The disappearance of the autochthonous meiofauna in the uppermost (6 m) sandy interval (Dasgupta *et al.*, 2020) testifies to the emersion of submarine bars.
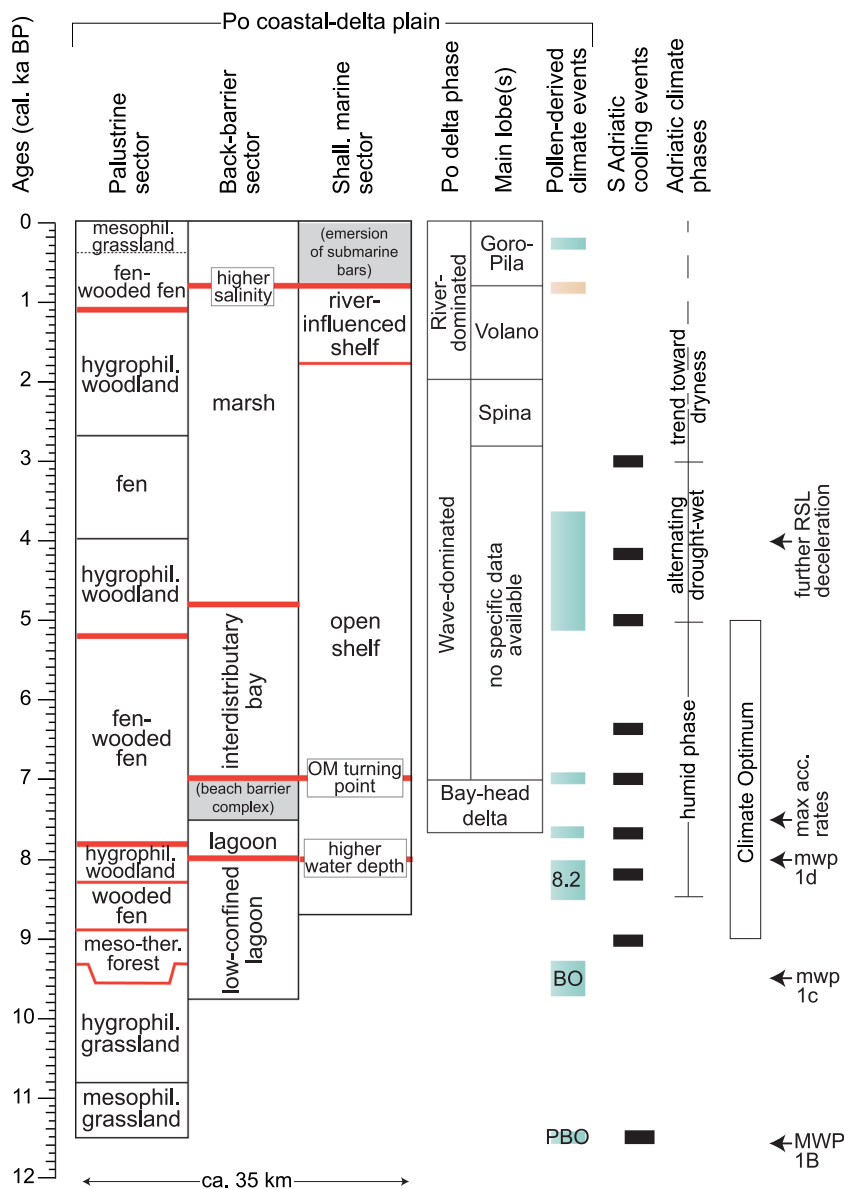
Figure 10. Summary diagram showing Holocene landscape changes and tipping points from the Po coastal-delta record, compared with published stratigraphic and palaeoclimate-RSL data. From left to right: stratigraphic succession of the ecosystems identified within the three sectors under examination (palustrine: core EM2; back-barrier: core 205 S5; shallow marine: core 205 S9; see Fig. 1 for location); Po Delta evolution phases as published in Correggiari *et al.* (2005) and Amorosi *et al.* (2019); palaeoclimate data from core EM2 (cool events are shown in blue, warm event in orange; Cacciari *et al.*, 2020); Adriatic palaeoclimate data derived from various geological archives including lacustrine and marine cored successions and speleothems (Wunsam *et al.*, 1999; Combourieu-Nebout *et al.*, 2013; Lončar *et al.*, 2017, 2019); glacio-eustatic data (Fairbanks, 1989; Liu *et al.*, 2004; Vacchi *et al.*, 2016). Main ecosystem shifts are highlighted in red. Red bold lines correspond to the landscape tipping points mentioned in the Discussion. [Color figure can be viewed at wileyonlinelibrary.com]

Back-barrier wetland

The back-barrier succession is composed of ~15-m-thick sand–silt deposits sandwiched by peaty, organic-rich clays (Fig. 3B). The basal peat (~22–21 m core depth), containing few specimens of the euryhaline foraminifer *A. tepida* (Table S1), is interpreted to have formed in the inner portion of the Po estuary during the earliest Holocene (~10 800–9750 cal a BP; Amorosi *et al.*, 2017; Bruno *et al.*, 2017). Upwards, the dominance of clusters F2 and O1 (>86 and 100%, respectively) along with the occurrence of Miliolids testifies to the establishment of a low-confinement lagoon ecosystem in an outer estuary (Fig. 8). The meiofauna palaeocommunity structure and DC1 sample scores record frequent variations in the rate of seawater exchange under rather stable (brackish) salinity conditions, suggesting intense marine processes by waves and currents. Around 8000 cal a BP, the disappearance of Miliolids accompanied by more positive, uniform values of DC1 scores record a shift towards a less open environment under unchanged salinity conditions (lagoon ecosystem; Fig. 8). The superposition of beach-barrier sands records the maximum marine ingression at the study site around 7500 cal a BP (Figs. 2 and 8). At the renewal of back-barrier sedimentation, around 7000 cal a BP, the composition and structure of meiofauna communities testify to particular

environmental–ecological conditions that lasted two millennia (up to ~5000 cal a BP). The appearance of saltmarsh foraminifers (cluster F1) and the overwhelming dominance of opportunistic taxa tolerant to restricted organic-rich environments, such as *A. tepida*–*A. parkinsoniana* (cluster F2) and *C. torosa* (cluster O1), point to a brackish, tidally influenced basin with limited connection to the open sea (Fig. 8). The occasional occurrence of the mesohaline species *D. stevensoni* and DC1 scores suggest a significant decrease in salinity relative to the earlier lagoonal ecosystems, reflecting an increase in fluvial influence.

All these features testify to the establishment of a wide bay (or a set of closely spaced embayments) with several outlets distributed over more than 30 km of the coastline (Amorosi *et al.*, 2019) and surrounded by freshwater wetlands. These embayments were mainly fed by longshore currents via tidal inlets and a network of tidal channels and tidal creeks that probably reduced their sediment transport after ~6000 cal a BP (Giacomelli *et al.*, 2018), as suggested by the estimated accumulation rates (Figs. 3B and 8).

The abrupt superposition of peaty clays dated to around 5000–4800 cal a BP is paralleled by a marked turnover in the meiofauna (Fig. 8), which sees the disappearance of foraminifers and the growth of hypohaline ostracods commonly thriving in standing-waters with phytal bottoms (cluster

O2 > 95%; Table 3). This sudden shift towards marshland conditions reasonably reflects an approaching Po river branch that contributed significantly to lower salinity (highly positive DC1 scores; Fig. 10). Atop, the sudden recovery of brackish ostracods (cluster O1 ~95%; Table 3) and the renewed appearance of foraminifers (cluster F2) are interpreted as an environmental–ecological change forced by a recent flooding event, well documented across the Po coastal plain (Fig. 2; Amorosi *et al.*, 2017).

Palustrine sector

At the beginning of the Holocene (~11 500 cal a BP), a mesophilous grassland (low tree cover and dominance of cluster P3: ~60%) colonized the innermost portion of the study area (Fig. 9). Around 10 800 cal a BP the replacement of cluster P3 by P1 and P4 taxa, which peak together at ~40%, points to the development of a hygrophilous grassland under a rising water table (Fig. 9). Then, an abrupt vegetation change occurred around 9300 cal a BP, with the establishment of a meso-thermophilous forest (dominance of cluster P5 ~60%) documenting a low degree of disturbance (negative DC1 scores) and moderate soil humidity (P1 taxa at ~20%). This peculiar forest ecosystem reflects the recolonization of the Po Plain by oak and related tree taxa that moved away from the central Italy Adriatic refugia since the Boreal period (Accorsi *et al.*, 1996). A few centuries later (around 9000 cal a BP), the forest was substituted by a more open, disturbed (DC1 scores around zero) vegetation typical of a wooded fen with dominant P1 taxa (~30–50%; Fig. 9). This shift reflects widespread drowning of the plain, accompanied by increased OM accumulation (i.e. organic-rich clays; Figs. 3C and 9). Around 8300 cal a BP, the sudden drop in P1 taxa accompanied by willow wood expansion (P2 up to 30%) points to the local development of hygrophilous woodlands, thriving the reliefs formed by repeated overbank events that affected the site up to ~8000–7800 cal a BP (Fig. 9). This change in environmental–depositional conditions is further highlighted by an increase in both grain size (from organic clays to sand–silt) and accumulation rates (from ~0.1 to 0.6 cm a^{-1}; Fig. 3C).

The following recovery of P1 taxa (ranging most often around 60%) and the marked decrease in tree cover (<20%) point to the development of a fen environment. Between 7800 and 5000 cal a BP, the high-frequency alternation of fen–wooded fen is interpreted to reflect the persistence of flooded, peaty areas (i.e. fen) that were periodically and partially filled (i.e. wooded fen) via overbank processes (Fig. 9). However, the intensity of fluvial activity and its effect on the vegetation were lower than in the period 8300–7800 cal a BP, as documented by the reduced thickness of overbank deposits and the overall decrease in accumulation rates, especially after 7300 cal a BP (Fig. 3C).

The abrupt superposition of a 3-m-thick sand–silt interval, encompassing ~1000 years (~5000–4000 cal a BP), is paralleled by another vegetation shift towards hygrophilous woodlands (i.e. high tree cover and negative DC1 scores). This was due to a renewed phase of high fluvial activity, followed by the re-establishment of a fen environment (Fig. 9). A similar vegetation pattern, from hygrophilous woodland to fen, is recorded between ~2700 and 1100 cal a BP. The recent development of a wooded fen abruptly turning into a highly disturbed (i.e. high DC1 scores) mesophilous grassland reflects draining and emergence of the plain, mainly due to anthropic land reclamation.

Holocene landscape changes: tipping points and drivers

The Holocene sedimentary evolution of the Po coastal plain has been reconstructed on the basis of sediment core analysis corroborated by hundreds of radiocarbon dates (Amorosi *et al.*, 2017, 2019; Bruno *et al.*, 2017; Campo *et al.*, 2017).

Despite the bias and the margin of error introduced by the application of age–depth models on different (transitional to shallow-marine) successions, the combination of bio-sedimentary records documents substantial coeval ecosystem shifts along a 35-km-long transect (Fig. 1). These turnovers provide a sound record of the Holocene dynamics occurring in microtidal coastal settings.

The most significant and widespread changes date to around 8000/7800, 7000, 4800/5000 and 1100/800 cal a BP (Fig. 10) and mark the major tipping points of the landscape during the Holocene. These critical thresholds, which pushed the Po coastal system into new, temporary stable states, allow us to define five environmental–ecological stages discussed below in the frame of previous stratigraphic reconstructions (Fig. 11).

11 500–8000 cal a BP: backstepping wave-dominated estuary surrounded by hygrophilous areas (Fig. 11A)

The ecological succession of mesophilous grassland–hygrophilous grassland–wooded fen at the landward margin of the Po estuary testifies to a progressive increase in soil humidity (i.e. rising water table), between ~11 500 and 8300 cal a BP (Figs. 9 and 10). This trend suggests that rapid RSL rise in the early Holocene period (Vacchi *et al.*, 2016), enhanced by subsidence, played a major role in paludal growth via prolonged seasonal soil waterlogging. Abrupt changes in the composition and structure of the local vegetation occurred during this time interval in response to two high-magnitude, well-known climate changes: the onset of the Holocene Climate Optimum and the 8200 event (Bond *et al.*, 1997). The former event drove the temporary expansion of mixed oak forests associated with Potential Natural Vegetation achievement (Cacciari *et al.*, 2020); the latter induced a long-lasting period of increased fluvial activity favouring the establishment of a humid, riparian woodland (Fig. 10).

Low confined lagoon and open-shelf ecosystems developed at more distal locations. Both ecosystems were seemingly insensitive to the highly variable climate–eustatic conditions of the early Holocene (Figs. 7, 8 and 10). The highly condensed sedimentary record of the marine sector, with a relatively poor stratigraphic resolution (Fig. 3A, B), can partly account for the record of such a stable ecosystem state. The low degree of confinement of the back-barrier sector associated with its high water salinity (Fig. 8) coherently reflects active meteo-marine conditions under continued RSL rise.

8000–7000 cal a BP: Prograding bay–delta system with peatlands (Fig. 11B)

Between 8000 and 7800 cal a BP, a major change in coastal landscape occurred with the development of permanently saturated wetlands or peatlands (i.e. fen–wooded fen vegetation), passing seaward to restricted lagoonal areas, replaced in turn by a beach–barrier system in the final stages of the Holocene transgression (Figs. 8–10). At the same time, increasing water depths modified the shelf meiofauna, which also shows abundant epiphytic taxa indicative of typically low fluvially influenced conditions (Figs. 7 and 10). Accelerating RSL rise at the time of maximum marine ingression (meltwater pulse - mwp 1d and maximum rising rates; Liu *et al.*, 2004;
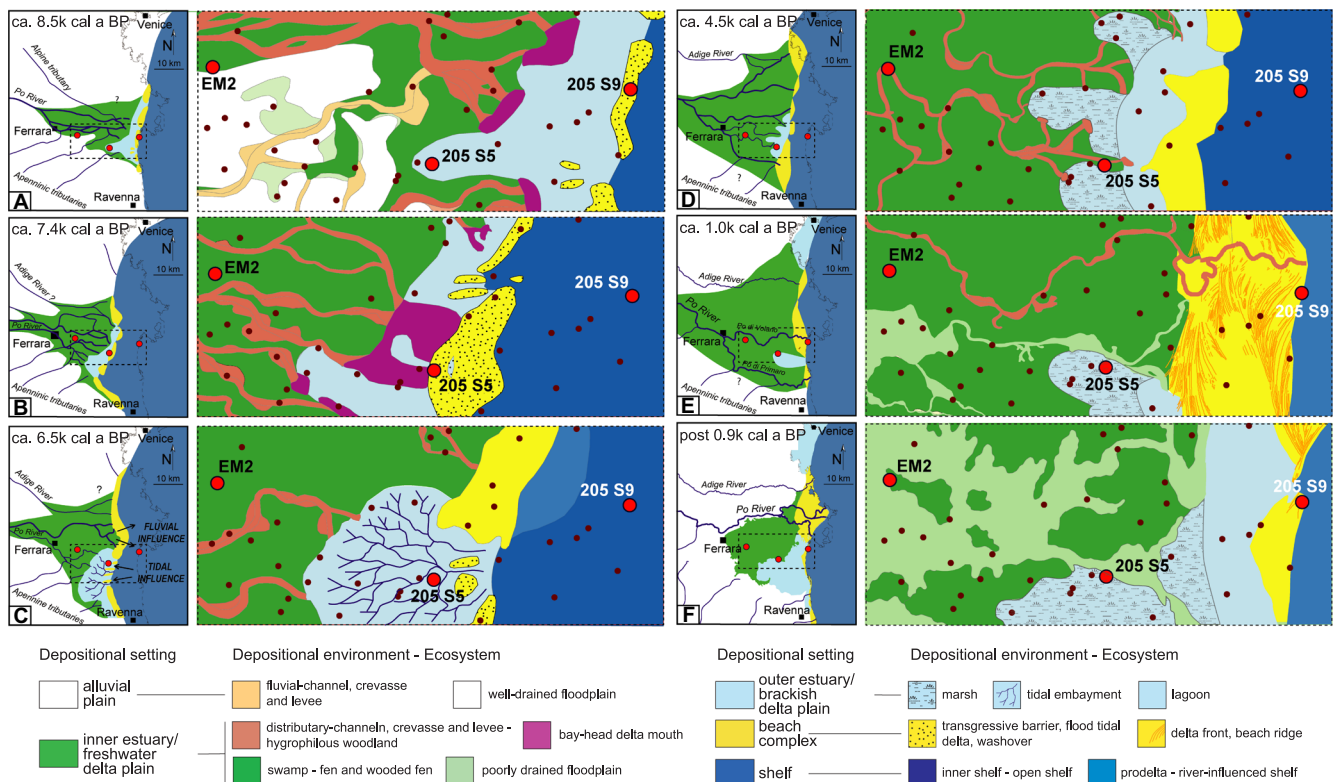
Figure 11. Palaeogeographical reconstruction showing Holocene landscape changes during the Holocene period (A–F) in the study area. Ages are reported as calibrated years BP. Reference cores analysed in this study are highlighted. Small, dark red points indicate other sedimentary cores used for map construction. Beach ridge traces (E) are from Regione Emilia-Romagna (https://dati.emilia-romagna.it/dataset). A, B and C are slightly modified from Amorosi et al. (2017). [Color figure can be viewed at wileyonlinelibrary.com]

Vacchi et al., 2016) represented the main forcing factor. A worldwide deceleration in RSL since ~7500 cal a BP then triggered the progradation of a confined bay–delta system (sensu Simms et al., 2018). The seaward migration of coastal environments co-determined ecosystem shifts into the Po estuary, which progressively turned into a wide, stagnant wetland. Evident environmental–ecological impact linked to the Adriatic cooling events centred on 7700 and 7000 cal a BP (Combourieu-Nebout et al., 2013; Cacciari et al., 2020) has not been recorded. However, we cannot exclude that climate instability correlated to these events increased river inputs and accelerated bay–delta progradation, as identified in other parts of the Adriatic Basin (Combourieu-Nebout et al., 2013).

7000-4800 cal a BP: Tidally influenced bay surrounded by peatlands (Fig. 11C)

Around 7000 cal a BP, ecosystem shifts in both back-barrier and marine sectors document the establishment of an open-sea landscape with a wide bay, colonized by saltmarsh foraminifers and opportunistic, euryhaline taxa (Fig. 8). A slight increase in opportunistic, OM-tolerant taxa typified the coeval shelf in response to the advent of riverine fluxes. The establishment of a tidally influenced bay surrounded by peatlands was reasonably triggered by the northward switching of the Po delta lobes. The long-term persistence of these conditions was favoured by a peculiar eustatic and climate context. Indeed, the high sea levels (i.e. the Holocene highstand) accompanied by relatively stable climate-optimum, humid conditions (Wunsam et al., 1999; Lončar et al., 2019; Fig. 10) worked together guaranteeing a high water table.

4800–800 cal a BP: Delta plain with brackish wetlands surrounded by wooded peatlands (Fig. 11D-E)

Unstable climate conditions, including high-frequency cooling events and alternating drought–wet phases followed by a drying trend (Combourieu-Nebout et al., 2013; Lončar et al., 2019), played a major role as disturbance on the late Holocene landscape. Climate variability influenced fluvial regimes in terms of floods (Macklin and Lewin, 2003; Benito et al., 2015), sediment production–downstream delivery (Fletcher and Zielhofer, 2013; Sarti et al., 2015) and delta lobe switching (Chadwick and Lamb, 2019). Changes in river flow regime and longshore sediment transport, corroborated by a further deceleration in RSL at ~4000 cal a BP (Vacchi et al., 2016), enhanced the progradation of the Po delta system and promoted reworking of sands at distributary channel mouths by sea currents. These processes triggered the bay's isolation from the sea and its transformation into stagnant, low-brackish marshlands, colonized exclusively by hypohaline ostracods. Accordingly, a wooded peatland developed landward, with the patchy occurrence of hygrophilous woodlands that colonized the overbank reliefs formed during periods of intense fluvial activity (Figs. 9 and 10). Seaward, the activation of new lobes (specifically the Volano lobe; Figs. 1 and 10) determined a marked turnover in the foraminiferal fauna with the dominance of opportunistic species able to tolerate remarkable OM riverine fluxes (Fig. 7). Although anthropogenic indicators in pollen diagrams are almost absent (Cacciari et al., 2020), we cannot rule out that changes in land use (i.e. deforestation, pastoralism, agriculture activities) cooperated to increase sediment fluxes to the sea, especially since the Roman period (i.e. river-dominated delta sensu Amorosi et al., 2019; Fig. 10).

800 cal a BP to present: Sediment-starved delta plain, reclaimed wetlands (Fig. 11F)

The occurrence of higher salinity conditions, tracked by the meiofauna in the back-barrier sector (Figs. 8 and 10), and the landward re-establishment of a fen–wooded fen environment point to a flooding event, which occurred during Medieval times in response to the Po River avulsion in Ficarolo, NW of Ferrara (Fig. 1). This avulsion, whose causes are still under discussion (climate fingerprint?; Veggiani, 1985, 1990), shifted the delta system towards its present-day position in the north (Fig. 1), leading to the abandonment of the Volano lobe and causing sediment starvation in the study area (Giacomelli et al., 2018). Recent reclamation works have resulted in the draining of submerged wetlands and the abrupt development of a highly disturbed mesophilous grassland in place of fen–wooded fen (Figs. 9 and 10).

Conclusions

The multi-proxy, stratigraphically based study of the Holocene succession of the Po Plain, built on the combination of benthic foraminifers, ostracods, palynomorphs and radiocarbon dating, revealed a set of millennial-scale variations in microtidal ecosystems along a 35-km-long, sea–land transect. Within three distinct sectors of the plain (i.e. palustrine, back-barrier and shallow-marine environments), bio-sedimentary data and their multivariate elaboration (CA and DCA) allowed identifying ecosystem dynamics and their driving parameters guided, in turn, by trends in RSL, climate and fluvial activity. On a broader perspective, such a variability reflects an evolving coastal landscape through the overcoming of successive critical thresholds.

Our data and interpretations support the following conclusions:

- If placed into a high-resolution stratigraphic framework, the multivariate (CA and DCA) palaeoecological approach is successful in documenting ecosystem responses of microtidal coastal areas to past perturbations. Through the Holocene period, the composition and structure of meiofauna palaeocommunities track variations in OM–water depth and degree of confinement–salinity within shallow-marine and back-barrier settings, respectively. Pollen and spores from freshwater palustrine successions proved to be even more sensitive than the meiofauna in the face of disturbance factors, highlighting several shifts in local vegetation associated with an oscillating water table and unsteady fluvial activity.
- In the shallow-marine sector, delta dynamics outweighed RSL in controlling the main ecosystem turnover on the inner shelf during the last ~8500 years. At the opposite edge of the coastal transect, within the freshwater palustrine sector, shifts were associated with RSL trends and climate oscillations. RSL rise influenced water table conditions, leading to the development of a peatland at the time of its maximum acceleration (~8000–7800 cal a BP). Cooling oscillations mainly acted via increasing fluvial activity, which resulted in peculiar morphologies and substrates (i.e. overbank sand–silt bodies) locally favouring riparian trees.
- Within the back-barrier sector, the combined effect of RSL and climate changes guided ecosystem variability from a low confined lagoon to a more restricted, brackish basin. The open lagoon was associated with intense meteo-marine conditions that occurred under rapid rising sea levels. Under relatively stable high sea levels (i.e. < 7000 cal a BP), unchanging climate conditions probably favoured the persistence of wide embayments in the delta plain. By contrast, the occurrence of a mid–late Holocene climate variability since ~5000 cal a BP is coeval with bays transformating into brackish wetlands.

- Four main tipping points, highlighting changes in the landscape overtime, are recognized at ~8000, 7000, 4800 and 800 cal a BP. Two of them (8000 and 4800 cal a BP) are related to major variations in RSL rising trends (acceleration versus deceleration) and in climate conditions that in turn influenced fluvial activity across the plain. The one at 7000 cal a BP was found to be associated with progradation of a confined bay–delta system (i.e. the filling of the Po estuary) at the turnaround from transgression to regression (~7500–7000 cal a BP). The youngest threshold (1100 BP/ 800 cal a BP) is connected with a major avulsion of the Po River, whose triggering factor(s) is still under debate.

Supporting Information

Table S1. Raw dataset used in this paper. Counts of benthic foraminifer, ostracod and pollen taxa are reported for the studied cores (205 S9, 205 S5 and EM2). Samples barren of autochthons fossils are not shown. Fossil identification guidelines and papers dealing with species ecological characterization are also shown.

Table S2. Dataset used for statistical analyses (CA and DCA).

Appendix S1. Settings of age–depth models.

Appendix S2. Biplot of DCA sample scores for the studied cores (BF: benthic foraminifers; O: ostracods).

Appendix S3. Dendrograms of the stratigraphically constrained cluster analysis (CONISS) and related broken stick plots for the studied cores (BF: benthic foraminifers; O: ostracods).

Data availability statement

The data that support the findings of this study are available in the Supporting Information.

Supporting information

Additional supporting information can be found in the online version of this article.

Table S1. Raw dataset used in this paper. Counts of benthic foraminifer, ostracod and pollen taxa are reported for the studied cores (205 S9, 205 S5 and EM2). Samples barren of autochthons fossils are not shown. Fossil identification guidelines and papers dealing with species ecological characterization are also shown.

Table S2. Dataset used for statistical analyses (CA and DCA).

Appendix S1. Settings of age–depth models.

Appendix S2. Biplot of DCA sample scores for the studied cores (BF: benthic foraminifers; O: ostracods).

Appendix S3. Dendrograms of the stratigraphically constrained cluster analysis (CONISS) and related broken stick plots for the studied cores (BF: benthic foraminifers; O: ostracods).

Abbreviations. AMS, accelerator mass spectrometry; CA, cluster analysis; DCA, detrended correspondence analysis; OM, organic matter; RSL, relative sea level.

References

Accorsi CA, Bandini Mazzanti M, Forlani L et al. 1999. An overview of Holocene forest pollen flora/vegetation of the Emilia Romagna region Northern Italy. Archivio Geobotanico 5: 3–27.

Accorsi CA, Bandini Mazzanti M, Forlani L et al. 2004. Holocene forest vegetation (pollen) of the Emilia Romagna plain – northern Italy. In La végétation postglaciaire du passé et du présent, Pedrotti F, Gehu JM (eds). Colloq. Phytosociol. 28: 1–103.

Accorsi CA, Bandini Mazzanti M, Mercuri AM et al. 1996. Holocene forest pollen vegetation of the Po Plain – Northern Italy (Emilia Romagna Data). Allionia 34: 233–275.

Alizad K, Hagen SC, Medeiros SC et al. 2018. Dynamic responses and implications to coastal wetlands and the surrounding regions under sea level rise. PLoS ONE 13: e0205176.

Amorosi A, Barbieri G, Bruno L et al. 2019. Three-fold nature of coastal progradation during the Holocene eustatic highstand, Po Plain, Italy – close correspondence of stratal character with distribution patterns. Sedimentology 66: 3029–3052.

Amorosi A, Bracone V, Campo B et al. 2016. A late Quaternary multiple paleovalley system from the Adriatic coastal plain (Biferno River, Southern Italy). Geomorphology 254: 146–159.

Amorosi A, Bruno L, Campo B et al. 2017. Global sea-level control on local parasequence architecture from the Holocene record of the Po Plain, Italy. Marine and Petroleum Geology 87: 99–111.

Amorosi A, Centineo MC, Colalongo ML et al. 2003. Facies architecture and Latest Pleistocene–Holocene depositional history of the Po Delta (Comacchio Area), Italy. Journal of Geology 111: 39–56.

Amorosi A, Rossi V, Scarponi D et al. 2014. Biosedimentary record of postglacial coastal dynamics: high-resolution sequence stratigraphy from the northern Tuscan coast (Italy). Boreas 43: 939–954.

Aucelli PPC, Di Paola G, Rizzo A et al. 2018. Present day and future scenarios of coastal erosion and flooding processes along the Italian Adriatic coast: the case of Molise region. Environmental Earth Sciences 77: 371.

Azzarone M, Pellegrini C, Barbieri G et al. 2020. Linking benthic fauna and seismic facies to improve stratigraphic reconstructions: the case of the mid-Adriatic deep since the late glacial period (central Adriatic sea). Bollettino della Società Paleontologica Italiana 59: 9–23.

Balbo AL, Martinez-Fernández J, Esteve-Selma M-A. 2017. Mediterranean wetlands: archaeology, ecology, and sustainability. Wiley Interdisciplinary Reviews: Water 4: e1238.

Barbieri G, Rossi V, Vaiani SC et al. 2019. Benthic ostracoda and foraminifera from the north Adriatic Sea (Italy, Mediterranean Sea): A proxy for the depositional characterisation of river-influenced shelves. Marine Micropaleontology 153.

Belanger CL, Garcia MV. 2014. Differential drivers of benthic foraminiferal and molluscan community composition from a multivariate record of early Miocene environmental change. Paleobiology 40: 398–416.

Bellotti P, Calderoni G, Dall'Aglio PL et al. 2016. Middle-to late-Holocene environmental changes in the Garigliano delta plain (Central Italy): which landscape witnessed the development of the Minturnae Roman colony? Holocene 26: 1457–1471.

Benito G, Macklin MG, Panin A et al. 2015. Recurring flood distribution patterns related to short-term Holocene climatic variability. Scientific Reports 5: 16398.

Benito X, Trobajo R, Cearreta A et al. 2016. Benthic foraminifera as indicators of habitat in a Mediterranean delta: implications for ecological and palaeoenvironmental studies. Estuarine, Coastal and Shelf Science 180: 97–113.

Bennett KD. 1996. Determination of the number of zones in a biostratigraphical sequence. New Phytologist 132: 155–170.

Bernhard JM, Sen Gupta BK, Borne PF. 1997. Benthic foraminiferal proxy to estimate dysoxic bottom-water oxygen concentrations; Santa Barbara Basin, U.S. Pacific continental margin. Journal of Foraminiferal Research 27: 301–310.

Bertini A, Ciaranfi N, Marino M et al. 2010. Proposal for Pliocene and Pleistocene land-sea correlation in the Italian area. Quaternary International 219: 95–108.

Blaauw M, Christen JA. 2011. Flexible paleoclimate age-depth models using an autoregressive gamma process. Bayesian Analysis 6: 457–474.

Blasi C, Capotorti G, & Copiz, R et al. 2014. Classification and mapping of the ecoregions of Italy. Plant Biosystems 148: 1255–1345.

Bonaduce G, Ciampo G, Masoli M. 1975. Distribution of Ostracoda in the Adriatic Sea. Pubblicazioni della Stazione Zoologica di Napoli. Olschki L. S., Napoli, Italy.

Bond G, Showers W, Cheseby M. 1997. A pervasive millennial-scale cycle in North Atlantic Holocene and glacial climates. Science 278: 1257–1266.

Bondesan M, Favero V, Viñals MJ. 1995. New evidence on the evolution of the Po-delta coastal plain during the Holocene. Quaternary International 29–30: 105–110.

Boomer I, Eisenhauer G. 2002. Ostracod faunas as palaeoenvironmental indicators in marginal marine environments. In The Ostracoda: Applications in Quaternary Research, Holmes JA, Chivas AR (eds). Geophysical Monograph Series: 135–149.

Breman E. 1975. The distribution of Ostracodes in the bottom sediments of the Adriatic Sea PhD Thesis, Free University of Amsterdam.

Bruno L, Bohacs KM, Campo B et al. 2017. Early Holocene transgressive palaeogeography in the Po coastal plain (northern Italy). Sedimentology 64: 1792–1816.

Bruno L, Campo B, Costagli B et al. 2020. Factors controlling natural subsidence in the Po Plain. Proceedings of the International Association of Hydrological Sciences 382: 285–290.

Buzas MA. 1990. Another look at confidence limits for species proportions. Journal of Paleontology 64: 842–843.

Cacciari M, Amorosi A, Marchesini M et al. 2020. Linking Holocene vegetation dynamics, palaeoclimate variability and depositional patterns in coastal successions: insights from the Po Delta plain of northern Italy. Palaeogeography, Palaeoclimatology, Palaeoecology 538.

Campo B, Amorosi A, Vaiani SC. 2017. Sequence stratigraphy and late Quaternary paleoenvironmental evolution of the northern Adriatic coastal plain (Italy). Palaeogeography, Palaeoclimatology, Palaeoecology 466: 265–278.

Campo B, Bohacs KM, Amorosi A. 2020. Late Quaternary sequence stratigraphy as a tool for groundwater exploration: lessons from the Po River Basin (northern Italy). AAPG Bulletin 104: 681–710.

Cearreta A, Benito X, Ibáñez C et al. 2016. Holocene palaeoenvironmental evolution of the Ebro Delta (western Mediterranean Sea): evidence for an early construction based on the benthic foraminiferal record. Holocene 26: 1438–1456.

Chadwick AJ, Lamb MP. 2019. Climate-change controls on river delta avulsion location & frequency. American Geophysical Union, Fall Meeting.

Ciabatti M. 1967. Ricerche sull'evoluzione del Delta Paedono. Giornale di Geologia 34: 381–406.

Coccioni R. 2000. Benthic foraminifera as bioindicators of heavy metal pollution – a case study from the Goro Lagoon (Italy). In Environmental Micropaleontology: the Application of Microfossils to Environmental Geology, Martin RE (ed.). Kluwer Academic Publishers/Plenum Press: New York; 71–103.

Combourieu-Nebout N, Peyron O, Bout-Roumazeilles V et al. 2013. Holocene vegetation and climate changes in the central Mediterranean inferred from a high-resolution marine pollen record (Adriatic Sea). Climate of the Past 9: 2023–2042.

Correa Metrio A, Dechnik Y, Lozano García S et al. 2014. Detrended correspondence analysis: A useful tool to quantify ecological changes from fossil data sets. Boletín de la Sociedad Geológica Mexicana 66: 135–143.

Correggiari A, Cattaneo A, Trincardi F. 2005. Depositional patterns in the late Holocene Po delta system. SEPM Special Publications 83: 365–392.

Cremonini S, Etiope G, Italiano F et al. 2008. Evidence of possible enhanced peat burning by deep-origin methane in the Po River delta plain (Italy). Journal of Geology 116: 401–413.

Cronin TM, DeMartino DM, Dwyer GS et al. 1999. Deep-sea ostracode species diversity: response to late Quaternary climate change. Marine Micropaleontology 37: 231–249.

D'Orefice M, Bellotti P, Bertini A et al. 2020. Holocene evolution of the Burano PaleoLagoon (Southern Tuscany, Italy). *Water (Switzerland)* **12**: 1–22.

Dasgupta U, Barbieri G, Vaiani SC et al. 2020. Potential and limits of benthic foraminiferal ecological indices in paleoenvironmental reconstructions: A case from a Holocene succession of the Po Delta, Italy. *Micropaleontology* **66**: 103–126.

Debenay J-P. 2000. Distribution trends of foraminiferal assemblages in paralic environments: a base for using foraminifera as bioindicators. In *Environmental Micropaleontology: the Application of Microfossils to Environmental Geology*, Martin RE (ed.). Kluwer Academic Publishers/Plenum Press, New York; 39–67.

Debenay JP, Guillou JJ. 2002. Ecological transitions indicated by foraminiferal assemblages in paralic environments. *Estuaries* **25**: 1107–1120.

Di Rita F, Celant A, Milli S et al. 2015. Lateglacial-early Holocene vegetation history of the Tiber delta (Rome, Italy) under the influence of climate change and sea level rise. *Review of Palaeobotany and Palynology* **218**: 204–216.

Donnici S, Serandrei Barbero R. 2002. The benthic foraminiferal communities of the northern Adriatic continental shelf. *Marine Micropaleontology* **44**: 93–123.

Ejarque A, Julià R, Reed JM et al. 2016. Coastal evolution in a Mediterranean microtidal zone: mid to late Holocene natural dynamics and human management of the Castelló Lagoon, NE Spain. *PLoS ONE* **11**: e0155446.

Fairbanks RG. 1989. A 17,000-year glacio-eustatic sea level record: influence of glacial melting rates on the Younger Dryas event and deep-ocean circulation. *Nature* **342**: 637–642.

Fletcher WJ, Zielhofer C. 2013. Fragility of western Mediterranean landscapes during Holocene Rapid Climate Changes. *CATENA* **103**: 16–29.

Frenzel P. 2019. Fossils of the southern Baltic Sea as palaeoenvironmental indicators in multi-proxy studies. *Quaternary International* **511**: 6–21 https://doi.org/10.1016/j.quaint.2018.09.014

Frenzel P, Boomer I. 2005. The use of ostracods from marginal marine, brackish waters as bioindicators of modern and Quaternary environmental change. *Palaeogeography, Palaeoclimatology, Palaeoecology* **225**: 68–92.

Frenzel P, Keyser D, Viehberg FA. 2010. An illustrated key and (palaeo)ecological primer for Postglacial to Recent Ostracoda (Crustacea) of the Baltic Sea. *Boreas* **39**: 567–575.

Frezza V, Carboni MG. 2009. Distribution of recent foraminiferal assemblages near the Ombrone River mouth (northern Tyrrhenian Sea, Italy). *Revue de Micropaléontologie* **52**: 43–66.

Giordana G, Rosenberg T, Spezzaferri S et al. 2011. Faunal evidence of a Holocene pluvial phase in southern arabia with remarks on the morphological variability of Helenina anderseni. *Journal of Foraminiferal Research* **41**: 248–259.

Ghilardi M, Delanghe D, Leandri F et al. 2017. Enregistrements d'événements extrêmes et évolution des paysages dans les basses vallées fluviales du Taravo et du Sagone (Corse occidentale, France) au cours de l'âge du Bronze moyen à final: une perspective géoarchéologique. *Géomorphologie: Relief, Processus, Environment* **23**: 15–35.

Giacomelli S, Rossi V, Amorosi A et al. 2018. A mid–late Holocene tidally influenced drainage system revealed by integrated remote sensing, sedimentological and stratigraphic data. *Geomorphology* **318**: 421–436.

Giaime M, Marriner N, Morhange C. 2019. Evolution of ancient harbours in deltaic contexts: A geoarchaeological typology. *Earth-Science Reviews* **191**: 141–167.

Gliozzi E, Grossi F. 2008. Late Messinian lago-mare ostracod palaeoecology: A correspondence analysis approach. *Palaeogeography, Palaeoclimatology, Palaeoecology* **264**: 288–295.

Grimm EC. 1987. CONISS: a FORTRAN 77 program for stratigraphically constrained cluster analysis by the method of incremental sum of squares. *Computers and Geosciences* **13**: 13–35.

Hayward BW, Scott GH, Grenfell HR et al. 2004. Techniques for estimation of tidal elevation and confinement (~salinity) histories of sheltered harbours and estuaries using benthic foraminifera: examples from New Zealand. *Holocene* **14**: 218–232.

Horne DJ, Curry BB, Mesquita-Joanes F. 2012. Mutual climatic range methods for Quaternary ostracods. In *Ostracoda as Proxies for Quaternary Climate Change. Developments in Quaternary Sciences*, Horne DJ, Holmes JA, Rodriguez-Lazaro J, Viehberg F (eds). Elsevier: Amsterdam; 65–84.

Horton BP, Edwards R. 2006. Quantifying Holocene sea level change using intertidal foraminifera: lessons from the British Isles. *Cushman Foundation for Foraminiferal Research Special Publication* **40**: 95.

Jongman R, Ter Braak C, Van Tongeren O, editors. 1995. *Data Analysis in Community and Landscape EcoLogy*. Cambridge University Press: Cambridge.

Jorissen F, Nardelli MP, Almogi-Labin A et al. 2018. Developing Foram-AMBI for biomonitoring in the Mediterranean: species assignments to ecological categories. *Marine Micropaleontology* **140**: 33–45.

Jorissen FJ. 1988. Benthic Foraminifera from the Adriatic Sea; principles of phenotypic variation. *Utrecht Micropaleontological Bulletins* **37**: 176.

Juggins S. 2020. *Rioja: Analysis of Quaternary Science Data*. R package version 0.9-26. https://cran.r-project.org/package=rioja

Kaniewski D, Marriner N, Morhange C et al. 2016. Solar pacing of storm surges, coastal flooding and agricultural losses in the Central Mediterranean. *Scientific Reports* **6**: 25197.

Kaniewski D, Marriner N, Morhange C et al. 2018. Holocene evolution of Portus Pisanus, the lost harbour of Pisa. *Scientific Reports* **8**: 11625.

Kaniewski D, Van Campo E, Guiot J et al. 2013. Environmental roots of the late Bronze Age crisis. *PLoS ONE* **8**: e71004.

Kassambara A, Mundt F. 2020. factoextra: extract and Visualize the Results of Multivariate Data Analyses. R package version 1.0.7. https://cran.r-project.org/package=factoextra

Langer MR. 1993. Epiphytic foraminifera. *Marine Micropaleontology* **20**: 235–265.

Langone L, Asioli A, Correggiari A et al. 1996. Age-depth modelling through the late Quaternary deposits of the central Adriatic Basin. *Memorie dell'Istituto italiano di idrobiologia* **55**: 177–196.

Laut LLM, Clemente IMMM, Belart P et al. 2016. Multiproxies (benthic foraminifera, ostracods and biopolymers) approach applied to identify the environmental partitioning of the Guadiana River Estuary (Iberian Peninsula). *Journal of Sedimentary Environments* **1**: 184–201.

Legendre P, De Cáceres M. 2013. Beta diversity as the variance of community data: dissimilarity coefficients and partitioning. *Ecology Letters* **16**: 951–963.

Legendre P, Gallagher ED. 2001. Ecologically meaningful transformations for ordination of species data. *Oecologia* **129**: 271–280.

Leorri E, Horton BP, Cearreta A. 2008. Development of a foraminifera-based transfer function in the Basque marshes, N. Spain: implications for sea-level studies in the Bay of Biscay. *Marine Geology* **251**: 60–74.

Leorri E, Martin R, McLaughlin P. 2006. Holocene environmental and parasequence development of the St. Jones Estuary, Delaware (USA): foraminiferal proxies of natural climatic and anthropogenic change. *Palaeogeography, Palaeoclimatology, Palaeoecology* **241**: 590–607.

Liu JP, Milliman JD, Gao S et al. 2004. Holocene development of the Yellow River's subaqueous delta, north Yellow Sea. *Marine Geology* **209**: 45–67.

Lončar N, Bar-Matthews M, Ayalon A et al. 2019. Holocene climatic conditions in the eastern Adriatic recorded in stalagmites from Strašna peć Cave (Croatia). *Quaternary International* **508**: 98–106.

Lowe JJ, Accorsi CA, & Bandini Mazzanti, M et al. 1996. Pollen stratigraphy of sediment sequences from carter lakes Albano and Nemi (near Rome) and from the central Adriatic, spanning the interval from oxygen isotope stage 2 to the present day. *Memorie dell'Istituto Italiano di Idrobiologia* **55**: 71–98.

Macklin MG, Lewin J. 2003. River sediments, great floods and centennial-scale Holocene climate change. *Journal of Quaternary Science* **18**: 101–105.

Magurran A. 2004. *Measuring Biological Diversity*. Blackwell Publishing Ltd: Oxford.

Mander L, Punyasena SW. 2018. Fossil pollen and spores in paleoecology. In *Methods in Paleoecology: Reconstructing Cenozoic Terrestrial Environments and Ecological Communities*, Croft DA, Su DF, Simpson SW (eds). Springer International Publishing: Cham; 215–234.

Masoli M. 1968. Ostracodi recenti dell'adriatico settentrionale tra Venezia e Trieste. *Memorie del Museo Tridentino di Scienze Naturali* **17**: 69–138.

Mazzini I, Rossi V, Da Prato S *et al*. 2017. Ostracods in archaeological sites along the Mediterranean coastlines: three case studies from the Italian Peninsula. *In The Archaeological and Forensic Applications of Microfossils: A Deeper Understanding of Human History*, Williams M, Hill T, Boomer I, Wilkinson IP (eds). Geological Society: London; 121–142.

Meisch C. 2000. Freshwater Ostracoda of Western and Central Europe. In *Süsswasserfauna von Mitteleuropa 8(3)*, Schwoerbel J, Zwick P (eds). Spektrum Akademischer Verlag: Heidelberg.

Melis R, Covelli S. 2013. Distribution and morphological abnormalities of recent foraminifera in the Marano and Grado Lagoon (north Adriatic Sea, Italy). *Mediterranean Marine Science* **14**: 432–450.

Melis RT, Di Rita F, French C *et al*. 2018. 8000 years of coastal changes on a western Mediterranean island: A multiproxy approach from the Posada plain of Sardinia. *Marine Geology* **403**: 93–108.

Milli S, Mancini M, Moscatelli M *et al*. 2016. From river to shelf, anatomy of a high-frequency depositional sequence: the Late Pleistocene to Holocene Tiber depositional sequence. *Sedimentology* **63**: 1886–1928.

Montenegro ME, Pugliese N. 1996. Autecological remarks on the ostracod distribution in the Marano and Grado lagoons (northern Adriatic Sea, Italy). *Bollettino della Società Paleontologica Italiana* **3**: 123–132.

Murray JW. 2006. *Ecology and Applications of Benthic Foraminifera.* Cambridge University Press: Cambridge.

Oksanen J, Blanchet G, Friendly M *et al*. 2019. Vegan: community ecology package. *R package version* **2**.5-6. https://cran.r-project.org/package=vegan

Pascual A, Rodriguez-Lazaro J, Martín-Rubio M *et al*. 2008. A survey of the benthic microfauna (foraminifera, Ostracoda) on the Basque shelf, southern Bay of Biscay. *Journal of Marine Systems* **72**: 35–63.

Perini L, Calabrese L, Luciani P *et al*. 2017. Sea-level rise along the Emilia-Romagna coast (Northern Italy) at 2100: scenarios and impacts. *Natural Hazards and Earth System Sciences Discussions*: 1–34.

Regione Emilia-Romagna. 1999. Carta Geologica della Pianura dell'Emilia-Romagna 1: 250,000.

Reimann L, Vafeidis AT, Brown S *et al*. 2018. Mediterranean UNESCO World Heritage at risk from coastal flooding and erosion due to sea-level rise. *Nature Communications* **9**: 4161.

Reimer PJ, Bard E, Bayliss A *et al*. 2013. IntCal13 and Marine13 radiocarbon age calibration curves 0–50,000 years cal Bp. *Radiocarbon* **55**: 1869–1887.

Revelles J, Ghilardi M, Rossi V *et al*. 2019. Coastal landscape evolution of Corsica island (W. Mediterranean): palaeoenvironments, vegetation history and human impacts since the early Neolithic period. *Quaternary Science Reviews* 225.

Richter Dde B, Billings SA. 2015. "One physical system": Tansley's ecosystem as Earth's critical zone. *New Phytologist* **206**: 900–912.

Rodríguez-Pérez A, Blázquez AM, Guillem J *et al*. 2018. Maximum flood area during MIS 1 in the Almenara marshland (western Mediterranean): benthic foraminifera and sedimentary record. *Holocene* **28**: 1452–1466.

Rogers K, Kelleway JJ, Saintilan N *et al*. 2019. Wetland carbon storage controlled by millennial-scale variation in relative sea-level rise. *Nature* **567**: 91–95.

Rossi V, Azzarone M, Capraro L *et al*. 2018. Dynamics of benthic marine communities across the Early-Middle Pleistocene boundary in the Mediterranean region (Valle di Manche, Southern Italy): biotic and stratigraphic implications. *Palaeogeography, Palaeoclimatology, Palaeoecology* **495**: 127–138.

Ruiz F, González-Regalado ML, Baceta JI *et al*. 2000. Los ostracodos actuales de la laguna de venecia (NE de Italia). *Geobios* **33**: 447–454.

Sacchi M, Molisso F, Pacifico A *et al*. 2014. Late-Holocene to recent evolution of Lake Patria, South Italy: an example of a coastal lagoon within a Mediterranean delta system. *Global and Planetary Change* **117**: 9–27.

Sadori L. 2013. Pollen records, postglacial, southern Europe. In *Encyclopedia of Quaternary Science*, 2nd edn, Elias SA (ed.). Elsevier: Amsterdam; 179–188.

Sadori L, Mazzini I, Pepe C *et al*. 2016. Palynology and ostracodology at the Roman port of ancient Ostia (Rome, Italy). *Holocene* **26**: 1502–1512.

Salel T, Bruneton H, Lefèvre D. 2016. Ostracods and environmental variability in lagoons and deltas along the north-western Mediterranean coast (Gulf of Lions, France and Ebro delta, Spain). *Revue de Micropaléontologie* **59**: 425–444.

Sarti G, Rossi V, Amorosi A *et al*. 2015. Climatic signature of two mid–late Holocene fluvial incisions formed under sea-level highstand conditions (Pisa coastal plain, NW Tuscany, Italy). *Palaeogeography, Palaeoclimatology, Palaeoecology* **424**: 183–195.

Scarponi D, Angeletti L. 2008. Integration of palaeontological patterns in the sequence stratigraphy paradigm: A case study from Holocene deposits of the Po Plain (Italy). *Geologica Acta* 7: 1–13.

Scarponi D, Azzarone M, Kusnerik K *et al*. 2017. Systematic vertical and lateral changes in quality and time resolution of the macrofossil record: insights from Holocene transgressive deposits, Po coastal plain, Italy. *Marine and Petroleum Geology* **87**: 128–136.

Scarponi D, Kaufman D, Amorosi A *et al*. 2013. Sequence stratigraphy and the resolution of the fossil record. *Geology* **41**: 239–242.

Schuerch M, Spencer T, Temmerman S *et al*. 2018. Future response of global coastal wetlands to sea-level rise. *Nature* **561**: 231–234.

Sedrati M, Ciavola P, Armaroli C. 2011. Morphodynamic evolution of a microtidal barrier, the role of overwash: bevano, northern Adriatic Sea. *Journal of Coastal Research* **64**: 696–700.

Seeliger M, Pint A, Feuser S *et al*. 2019. Elaia, Pergamon's maritime satellite: the rise and fall of an ancient harbour city shaped by shoreline migration. *Journal of Quaternary Science* **34**: 228–244.

Serandrei Barbero R, Albani AD, Bonardi M. 2004. Ancient and modern salt marshes in the Lagoon of Venice. *Palaeogeography, Palaeoclimatology, Palaeoecology* **202**: 229–244.

Shepard CC, Crain CM, Beck MW. 2011. The protective role of coastal marshes: A systematic review and meta-analysis. *PLoS ONE* **6**: e27374.

Simeoni U, Corbau C. 2009. A review of the Delta Po evolution (Italy) related to climatic changes and human impacts. *Geomorphology* **107**: 64–71.

Simms AR, Rodriguez AB, Anderson JB. 2018. Bayhead deltas and shorelines: insights from modern and ancient examples. *Sedimentary Geology* **374**: 17–35.

Slack JM, Kaesler RL, Kontrovitz M. 2000. Trend, signal and noise in the ecology of Ostracoda: information from rare species in low-diversity assemblages. *Hydrobiologia* **419**: 181–189.

Stanley DJ, Chen Z. 2000. Radiocarbon dates in China's Holocene Yangtze Delta: record of sediment storage and reworking, not timing of deposition. *Journal of Coastal Research* **16**: 1126–1132.

Stefani M, Vincenzi S. 2005. The interplay of eustasy, climate and human activity in the late Quaternary depositional evolution and sedimentary architecture of the Po Delta system. *Marine Geology* **222–223**: 19–48.

Tansley AG. 1935. The use and abuse of vegetational concepts and terms. *Ecology* **16**: 284–307.

R Core Team. 2019 *R: A Language and Environment for Statistical Computing.* R Foundation for Statistical Computing: Vienna.

Tsourou T. 2012. Composition and distribution of recent marine ostracod assemblages in the bottom sediments of central Aegean Sea (SE Andros island, Greece). *International Review of Hydrobiology* **97**: 276–300.

Vacchi M, Marriner N, Morhange C *et al*. 2016. Multiproxy assessment of Holocene relative sea-level changes in the western Mediterranean: sea-level variability and improvements in the definition of the isostatic signal. *Earth-Science Reviews* **155**: 172–197.

Van Der Zwaan GJ, Jorissen FJ. 1991. Biofacial patterns in river-induced shelf anoxia. *Geological Society, London, Special Publications* **58**: 65–82.

Veggiani A. 1985. *Il Delta del Po e l'evoluzione della rete idrografica padana in epoca storica*. Atti della Tavola Rotonda su Il Delta del Po, Bologna 24 Novembre 1982. Accademia delle Scienze dell'Istituto di Bologna, 37–68.

Veggiani A. 1990. Fluttuazioni climatiche e trasformazioni ambientali nel territorio imolese dall'alto medioevo all'età moderna. In *Imola Nel Medioevo*, Mancini F, Gioberti M, Veggiani A (eds). Imola, 41–102.

Vella MA, Andrieu-Ponel V, Cesari J *et al.* 2019. Early impact of agropastoral activities and climate on the littoral landscape of Corsica since mid-Holocene. *PLoS ONE* **14**: e0226358.

Wunsam S, Schmidt R, Müller J. 1999. Holocene lake development of two Dalmatian lagoons (Malo and Veliko Jezero, Isle of Mljet) in respect to changes in Adriatic sea level and climate. *Palaeogeography, Palaeoclimatology, Palaeoecology* **146**: 251–281.

Zampi M, D'Onofrio S. 1986. I foraminiferi della Laguna di Levante (Orbetello, Grosseto) *Atti della Società Toscana di Scienze Naturali, Memorie, Serie A* **93**: 101–127.

Zecchin M, Tosi L, Caffau M *et al.* 2014. Sequence stratigraphic significance of tidal channel systems in a shallow lagoon (Venice, Italy). *Holocene* **24**: 646–658.